Journal of Molecular Catalysis A: Chemical 397 (2015) 1–18

Contents lists available at ScienceDirect

Journal of Molecular Catalysis A: Chemical

journal homepage: www.elsevier.com/locate/molcata

Palladium nanoparticles encapsulated in a dendrimer networks as catalysts for the hydrogenation of unsaturated hydrocarbons

Edward A. Karakhanov[a,*], Anton L. Maksimov[a,b], Elena M. Zakharian[a], Yulia S. Kardasheva[a], Sergey V. Savilov[a], Nadezhda I. Truhmanova[b], Andrey O. Ivanov[b], Vladimir A. Vinokurov[c]

[a] Department of Chemistry, Lomonosov Moscow State University (MSU) , 119991 Moscow, Russia
[b] Institute of Petrochemical Synthesis RAS, 119991 Moscow, Russia
[c] I.M. Gubkin Russian State University of Oil and Gas, 119991 Moscow, Russia

ARTICLE INFO

Article history:
Received 24 July 2014
Received in revised form 14 October 2014
Accepted 15 October 2014
Available online 24 October 2014

Keyword:
Pd catalysts
Nanoparticles
PAMAM dendrimer
Selective hydrogenation

ABSTRACT

A novel method has been proposed for encapsulating palladium nanoparticles up to 5 nm in the matrix of polymeric support networks based on polyamidoamine dendrimers. The shape of the particle size distribution and the catalytic activity of the materials obtained during the hydrogenation of unsaturated compounds depend strongly on the support structure. High activity (TOF up to 86,000 h^{-1}) has been observed during the hydrogenation of styrene.

1. Introduction

Catalysts utilising metal nanoparticles as active components deposited on dendrimer matrices have recently found numerous applications in petrochemical and organic syntheses. These materials are used during the hydrogenation of double bonds [1], hydroformylation [2,3], amination [4], carbonylation [5] and cross-coupling reactions (the Suzuki [6], Heck [7] and the Sonogashira reaction [8]). The main problem with metal nanoparticles as catalysis is their aggregation, which leads to the decrease in the total specific surface of the catalyst and, as a consequence, to the activity loss. In a number of cases, the selectivity of the reaction also depends on the particle size. Metal nanoparticles can be stabilized by the interactions with either the donor atoms of various organic ligands following the coordination mechanism, or the internal surface of pores in such systems as zeolite and mesoporous aluminosilicates.

One of the most interesting approaches toward synthesising catalysts based on metal nanoparticles is the use of the dendrimers to bind metal ions, which are nanoparticle precursors, and to stabilise the resultant particles [9–12]. The dendrimer encapsulated nanoparticles have the advantage over other types of metaldendrite catalysts: the poly(propyleneimine) (PPI) and PAMAM dendrimers commonly used as a matrix can be relatively readily synthesized in laboratory from commercially available precursor [13–18]. We have proposed a method for synthesising a heterogeneous support based on polyamidoamine dendrimers, binding them to one another with special cross-linking agents, such as diisocyanates. It includes a preliminary cross-linking PPI- dendrimers with various bifunctional agents (diepoxides, diisocyanates) with subsequent deposition of a required metal salt and its reduction to the zerovalent state. The driving force for the preparation of the catalyst is the formation of the complex between the ions of the deposited metal and the amino groups of dendrimers. In this case, the final properties of the material (nanoparticle size distribution, catalytic activity and selectivity) are determined by the dendrimer generation, the size, rigidity, and polarity of the cross linking agent. Thus synthesized system structurally resembles metalorganic frameworks, in which the dendrimers, rather than metal ions, serve as the matrix nodes, whose rigidity increases with the increase in the generation and decrease in the length of the branches. Therefore, we prepared effective hydrogenation catalysts based on cross-linked dendrimers and palladium nanoparticles with particle sizes ranging from 1.8 to 2.8 nm based on generation of the PPI dendrimer [19]. The corresponding material exhibits a high activity when hydrogenating olefin and phenylacetylene [19–22]. In this paper,

* Corresponding author. Tel.: +7 495 939 53 77; fax: +7 495 939 19 51.
E-mail address: kar@petrol.chem.msu.ru (E.A. Karakhanov).

http://dx.doi.org/10.1016/j.molcata.2014.10.018
1381-1169/

we report the design of catalysts based on palladium nanoparticles and PAMAM dendrimers using the same approach.

2. Experimental

2.1. Analysis

The first-, second- and third-generation polyamidoamine dendrimers, specifically PAMAM-G1 (PAMAM $(NH_2)_8$), PAMAM-G2 (PAMAM $(NH_2)_{16}$), and PAMAM-G3 (PAMAM $(NH_2)_{32}$), were synthesised according to the procedure described in [23]; these materials were used as starting materials. The cross-linking agents, which were obtained from Aldrich, included the following: 1,4-butylene diisocyanate (BDI), 1,6-hexamethylene diisocyanate (HMDI), 1,8-octamethylene diisocyanate (OMDI), p-phenylene diisocyanate (PDI), and 3,3′-dimethoxy-4,4′-biphenylene diisocyanate (DMPDI).

The IR spectra were obtained with a Nicolet IR2000 (Thermo Scientific) using a method involving multiple distortions in the total internal reflection with Multi-reflection HATR accessories; these accessories contained a ZnSe crystal (45°) for use at different wavelengths and a resolution of 4 cm^{-1}.

The X-ray photoelectron spectroscopy (XPS) studies were performed with a Kratos Axis Ultra DLD electronic device equipped with a photoelectron analyser and an OPX-150 slowing potential. The photoelectrons were excited using X-rays from an aluminium anode (Al Kα = 1486.6 eV) at 12 kV and 20 mA. The photoelectron peaks were calibrated using the C 1s carbon line at 284.8 eV.

The palladium in the samples was quantified using inductively coupled plasma atomic emission spectroscopy (ICP-AES) with an IRIS Interpid II XPL instrument (Thermo Electron Corp., USA) through the radial and axial detection at 310 and 95.5 nm.

The transmission electron microscopy (TEM) studies of the samples were performed on a LEO912 AB OMEGA transmission electron microscope.

2.2. Synthesis of dendrimer compounds and characterization

Synthesis of PAMAM-G1-BDI. A 1.1-g portion of PAMAM$(NH_2)_8$ (0.773 mmol) and 50 mL of absolute THF were placed in a 100-mL single-neck flask equipped with a magnetic stirrer and a reflux condenser. Under these conditions, the dendrimer swelled but did not dissolve. Afterwards, 0.13 mL (1.031 mmol) of 1,4-butylene diisocyanate was added with stirring. The reaction proceeded for 12 h at 70 °C before the product mixture was evaporated in a rotary evaporator at 50 °C. The product was obtained as loose yellow lumps (1.357 mg).

Synthesis of PAMAM-G1-HMDI. The synthesis was carried out according to the procedure described above. The reactants included PAMAM$(NH_2)_8$ (1.088 g, 0.761 mmol) and 1,6-hexamethylene diisocyanate (0.16 mL, 1.014 mmol) in 50 mL of absolute THF. The reaction product was obtained as loose yellow lumps (1.259 g).

IR (sm^{-1}): 3302 (N-H_{st} in NH-C(=O)); 2933 (C-H_{st}); 2858 (C-H_{st}, CH_2-N_{st}); 1658 (C=O_{st} in NH-C(=O)); 1552 (N-H_δ, $CH_{2\delta}$, C-N-H_δ); 1477, 1433, 1387 ($CH_{2\delta}$); 1263, 1157, 1120, 1036 (C-N_{st} in NH-C(=O)).

Synthesis of PAMAM-G1-OMDI. The synthesis was carried out according to the procedure described above. The reactants included PAMAM$(NH_2)_8$ (0.568 g, 0.397 mmol) and 1,8-octamethylene diisocyanate (0.15 mL, 0.77 mmol) in 50 mL of absolute THF. The reaction product was obtained as yellow loose lumps (0.738 g).

Synthesis of PAMAM-G1-PDI. The synthesis was carried out according to the procedure described above. The reactants included PAMAM$(NH_2)_8$ (1.088 g, 0.761 mmol) and p-phenylene diisocyanate (0.65 g, 1.014 mmol) in 50 mL of absolute THF. The reaction product was obtained as a white powder (2.124 g).

IR (sm^{-1}): 3298 (N-H_{st} in NH-C(=O)); 2954 (C-H_{st}); 2843 (C-H_{st}, CH_2-N_{st}); 1633 (C=O_{st} in NH-C(=O)); 1558, 1510 (N-H_δ, $CH_{2\delta}$, C-N-H_δ); 1404, 1300 ($CH_{2\delta}$); 1219, 1126, 1072, 1016 (C-N_{st} in NH-C(=O)); 823 (aromatic C-H_δ); 761, 687, 652 (aromatic C=C_δ).

XPS (eV): 284.5 (32%), 285.7 (46%), 287.1 (8%), 288.5 (14%) (C 1s, 64.9%); 399.3 (N 1s, 22.1%); 530.8 (O 1s, 12.5%).

Synthesis of PAMAM-G1-DMPDI. The synthesis was carried out according to the procedure described above. The reactants included PAMAM$(NH_2)_8$ (1.871 g, 1.309 mmol) and 3,3′-dimethoxy-4,4′-diphenylene diisocyanate (0.518 g, 1.748 mmol) in 50 mL of absolute THF. The reaction product was obtained as loose white lumps (2.389 g).

IR (sm^{-1}): 3325 (N-H_{st} in NH-C(=O)); 2929 (C-H_{st}); 2856 (C-H_{st}, CH_2-N_{st}); 1628 (C=O_{st} in NH-C(=O)); 1547 (N-H_δ, $CH_{2\delta}$, C-N-H_δ); 1462, 1431 ($CH_{2\delta}$); 1261, 1119, 1038 (C-N_{st} in NH-C(=O)); 820 (aromatic C-H_δ); 768, 652 (aromatic C=C_δ).

Synthesis of PAMAM-G2-HMDI. The synthesis was carried out according to the procedure described above. The reactants included PAMAM$(NH_2)_{16}$ (2 g, 0.615 mmol) and 1,6-hexamethylene diisocyanate (0.26 mL, 1.64 mmol) in 50 mL of absolute THF. The reaction product was obtained as a yellowish sticky mass (2.011 g).

Synthesis of PAMAM-G2-PDI. The synthesis was carried out according to the procedure described above. The reactants included PAMAM$(NH_2)_{16}$ (2 g, 0.615 mmol) and p-phenylene diisocyanate (PDI) (0.262 g, 1.64 mmol) in 50 mL of absolute THF. The reaction product was obtained as a yellowish sticky mass (2.215 g).

Synthesis of PAMAM-G2-DMPDI. The synthesis was carried out according to the procedure described above. The reactants included PAMAM$(NH_2)_{16}$ (768 mg, 0.236 mmol) and 3,3′-dimethoxy-4,4′-diphenylene diisocyanate (711 mg, 2.4 mmol) in 50 mL of anhydrous methanol. The reaction product was obtained as a white powder (892 mg).

IR (sm^{-1}): 3325 (N-H_{st} in NH-C(=O)); 2929 (C-H_{st}); 2856 (C-H_{st}, CH_2-N_{st}); 1627, (C=O_{st} in NH-C(=O)); 1547 (N-H_δ, $CH_{2\delta}$, C-N-H_δ); 1462, 1431 $CH_{2\delta}$); 1261, 1157, 1113, 1038 (C-N_{st} in NH-C(=O)); 874, 820 (aromatic C-H_δ); 768, 729, 710, 658 (aromatic C=C_δ).

Synthesis of PAMAM-G3-HMDI. The synthesis was carried out according to the procedure described above. The reactants included PAMAM$(NH_2)_{32}$ (2 g, 0.29 mmol) and 1,6-hexamethylene diisocyanate (0.25 mL, 1.547 mmol) in 50 mL of absolute THF. The reaction product was obtained as a white powder (2.124 g).

IR (sm^{-1}): 3327 (N-H_{st} in NH-C(=O)); 2929 (C-H_{st}); 2854 (C-H_{st}, CH_2-N_{st}); 1628 (C=O_{st} in NH-C(=O)); 1556 (N-H_δ, $CH_{2\delta}$, C-N-H_δ); 1469, 1431, 1358 ($CH_{2\delta}$); 1261, 1153, 1037 (C-N_{st} in NH-C(=O)).

Synthesis of PAMAM-G3-PDI material. The synthesis was carried out according to the procedure described above. The reactants included PAMAM$(NH_2)_{32}$ (2 g, 0.29 mmol) and p-phenylene diisocyanate (PDI) (0.248 g, 1.57 mmol) in 50 mL of absolute THF. The reaction product was obtained as a white powder (2.549 g).

IR (sm^{-1}): 3327 (N-H_{st} in NH-C(=O)); 2916 (C-H_{st}); 2862 (C-H_{st}, CH_2-N_{st}); 1631 (C=O_{st} in NH-C(=O)); 1566 (N-H_δ, $CH_{2\delta}$, C-N-H_δ); 1477, 1433, 1335 ($CH_{2\delta}$); 1265, 1153, 1047 (C-N_{st} in NH-C(=O)); 904, 862, 827 (aromatic C-H_δ); 766, 669 (aromatic C=C_δ).

2.3. Preparation of Pd-dendrimer compounds and characterization

Synthesis of G1-BDI-Pd. To a 50-ml flask equipped with a magnetic stirrer and a reflux condenser was added 1.1 g of PAMAM-G1-BDI in 40 mL of absolute chloroform. Afterwards, 787 mg (3.51 mmol) of $Pd(OAc)_2$ was added to the resulting suspension with stirring. The reaction proceeded for 12 h at 70 °C.

After the reaction, the suspension was evaporated to dryness in a rotary evaporator. The intermediate product was a dark brown

powder (1.787 g, 100%). This material was placed in a 50-mL flask equipped with a magnetic stirrer and a reflux condenser before being suspended in a mixture containing 30 mL of chloroform and 10 mL of methanol. Sodium borohydride (1.334 g, 35.1 mmol) was added to the resulting suspension with stirring. The reaction mixture turned black, and a violent evolution of gas was observed. The reaction proceeded for 12 h at 60 °C. After the reaction, the suspension was evaporated to dryness in a rotary evaporator, and the resulting precipitate was washed twice with water and methanol before drying in air with heating. The product was obtained as a black powder (533 mg).

IR (sm^{-1}): 3334 (N-H_{st} in NH-C(=O)); 2922 (C-H_{st}); 2850 (C-H_{st}, CH_2-N_{st}); 1626 (C=O_{st} in NH-C(=O)); 1558, 1525 (N-H_δ, $CH_{2\delta}$, C-N-H_δ); 1477, 1435, 1356 ($CH_{2\delta}$); 1281, 1219, 1147, 1051 (C-N_{st} in NH-C(=O)).

XPS (eV): 284.7 (37.96%), 285.8 (40.22%), 286.1 (6.43%), 288.4 (15.4%) (C 1s, 64.5%); 335.0 (87%) (Pd $3d_{5/2}$, 4.7%), 337.9 (13%) (Pd $3d_{3/2}$); 399.5 (N 1s, 19.9%); 531.2 (O 1s, 10.9%). ICP-AES: 15.83% Pd.

Synthesis of G1-HMDI-Pd. The synthesis was carried out according to the procedure described above. The reactants included PAMAM-G1-HMDI (623 mg) and $Pd(OAc)_2$ (448 mg, 1.985 mmol) in 40 mL of absolute chloroform. The intermediate product was suspended in 30 mL of chloroform and 10 mL of methanol before adding sodium borohydride (757 mg, 19.85 mmol). The product was a black powder (275 mg).

IR (sm^{-1}): 3324 (N-H_{st} in NH-C(=O)); 2924 (C-H_{st}); 2852 (C-H_{st}, CH_2-N_{st}); 1624 (C=O_{st} in NH-C(=O)); 1554, 1523 (N-H_δ, $CH_{2\delta}$, C-N-H_δ); 1485, 1433, 1386 ($CH_{2\delta}$); 1254, 1149 (C-N_{st} in NH-C(=O)).

XPS (eV): 284.7 (40.1%), 285.7 (37.7%), 287.2 (11.9%), 288.3 (8.6%) (C 1s, 52.5%); 335.7 (62%) (Pd $3d_{5/2}$, 8.9%), 338.2 (38%) (Pd $3d_{3/2}$); 399.5 (N 1s, 13.8%); 531.1 (O 1s, 19.6%). ICP-AES: 14.8% Pd.

Synthesis of G1-OMDI-Pd. The synthesis was carried out according to the procedure described above. The reactants included PAMAM-G1-OMDI (738 mg) and $Pd(OAc)_2$ (246 mg, 1.097 mmol) in 40 mL of absolute chloroform. The intermediate product was suspended in 30 mL of chloroform and 10 mL of methanol before adding sodium borohydride (417 mg, 10.97 mmol). The product was a black powder (146 mg).

IR (sm^{-1}): 3307 (N-H_{st} in NH-C(=O)); 2939 (C-H_{st}); 2854 (C-H_{st}, CH_2-N_{st}); 1624 (C=O_{st} in NH-C(=O)); 1564, 1523 (N-H_δ, $CH_{2\delta}$, C-N-H_δ); 1433, 1360 ($CH_{2\delta}$); 1254, 1163, 1043 (C-N_{st} in NH-C(=O)).

XPS (eV): 284.6 (53.2%), 285.7 (30.34%), 286.6 (4.82%), 288.5 (11.64%) (C 1s, 61.7%); 335.2 (68%) (Pd $3d_{5/2}$, 1.2%), 338.0 (32%) (Pd $3d_{3/2}$); 399.5 (N 1s, 24.9%); 531.4 (O 1s, 12.2%). ICP-AES: 5.45% Pd.

Synthesis of G1-PDI-Pd. The synthesis was carried out according to the procedure described above. The reactants included PAMAM-G1-PDI (531 mg) and $Pd(OAc)_2$ (352 mg, 1.56 mmol) in 40 mL of absolute chloroform. The intermediate product was suspended in 30 mL of chloroform and 10 mL of methanol before adding sodium borohydride (595 mg, 15 mmol). The resulting product was a black powder (533 mg).

IR (sm^{-1}): 3319 (N-H_{st} in NH-C(=O)); 2925 (C-H_{st}); 2858 (C-H_{st}, CH_2-N_{st}); 1635 (C=O_{st} in NH-C(=O)); 1547, 1510 (N-H_δ, $CH_{2\delta}$, C-N-H_δ); 1448, 1404 ($CH_{2\delta}$); 1298, 1221, 1070, 1009 (C-N_{st} in NH-C(=O)); 849, 827 (C-H_δ in aromatic ring); 760, 644 (C=C_δ in aromatic ring).

XPS (eV): 284.4 (50.6%), 285.5 (33.2%), 286.8 (8.9%), 288.1 (7.4%) (C 1s, 65.9%); 335.7 (45%) (Pd $3d_{5/2}$, 3.9%), 338.2 (55%) (Pd $3d_{3/2}$); 399.5 (N 1s, 13.9%); 531.9 (O 1s, 13.0%). ICP-AES: 6.5% Pd.

Synthesis of G1-DMPDI-Pd. The synthesis was carried out according to the procedure described above. The reactants included PAMAM-G1-DMPDI (2.389 g) and $Pd(OAc)_2$ (0.978 g, 4.362 mmol) in 40 mL of absolute chloroform. The intermediate product was suspended in 30 mL of chloroform and 10 mL of methanol before adding sodium borohydride (1.66 g, 43.62 mmol). The product was a black powder (275 mg).

IR (sm^{-1}): 3250 (N-H_{st} in NH-C(=O)); 2918 (C-H_{st}); 2850 (C-H_{st}, CH_2-N_{st}); 1699, 1637 (C=O_{st} in NH-C(=O)); 1550, 1510 (N-H_δ, $CH_{2\delta}$, C-N-H_δ); 1439, 1390, 1321 ($CH_{2\delta}$); 1244, 1205, 1173, 1142, 1024 (C-N_{st} in NH-C(=O)); 949, 837, 814 (aromatic C-H_δ); 733, 654 (aromatic C=C_δ).

XPS (eV): 284.4 (43.78%), 285.7 (36.26%), 286.8 (8.23%), 288.3 (11.73%) (C 1s, 69.1%); 335.2 (83%) (Pd $3d_{5/2}$, 6.5%), 337.9 (17%) (Pd $3d_{3/2}$); 399.5 (N 1s, 14.6%); 531.2 (O 1s, 9.8%). ICP-AES: 13.12% Pd.

Synthesis of G2-HMDI-Pd. The synthesis was carried out according to the procedure described above. The reactants included PAMAM-G2-HMDI (300 mg) and $Pd(OAc)_2$ (48.6 mg, 0.216 mmol) in 30 mL of methylene chloride. The intermediate product was suspended in 30 mL of methylene chloride and 10 mL of methanol before adding sodium borohydride (82.4 mg, 2.16 mmol). The product was a black layered powder (130 mg).

IR (sm^{-1}): 3315 (N-H_{st} in NH-C(=O)); 2931 (C-H_{st}); 2860 (C-H_{st}, CH_2-N_{st}); 1624 (C=O_{st} in NH-C(=O)); 1550 (N-H_δ, $CH_{2\delta}$, C-N-H_δ); 1435, 1335 ($CH_{2\delta}$); 1261, 1068 (C-N_{st} in NH-C(=O)).

XPS (eV): 284.4 (64.1%), 285.5 (19.7%), 286.4 (8.7%), 288.1 (7.5%) (C 1s, 79.2%); 338.5 (Pd $3d_{3/2}$, 0.3%); 399.5 (N 1s, 3.3%); 531.5 (O 1s, 4.0%). ICP-AES: 1.61% Pd.

Synthesis of $G_2$2-HMDI-Pd. The synthesis was carried out according to the procedure described above. The reactants included PAMAM-G2-HMDI (500 mg), $Pd(OAc)_2$ (211 mg, 0.941 mmol) and sodium borohydride (357.6 mg, 9.41 mmol). The product was a black powder (114 mg).

IR (sm^{-1}): 3329 (N-H_{st} in NH-C(=O)); 2924 (C-H_{st}); 2856 (C-H_{st}, CH_2-N_{st}); 1620 (C=O_{st} в NH-C(=O)); 1549 (N-H_δ, $CH_{2\delta}$, C-N-H_δ); 1477, 1433 ($CH_{2\delta}$); 1242, 1072 (C-N_{st} in NH-C(=O)).

XPS (eV): 284.7 (82.58%), 285.6 (12.14%), 286.7 (2.7%), 288.3 (2.58%) (C 1s, 90.4%); 334.8 (50%) (Pd $3d_{5/2}$, 0.3%), 337.9 (50%) (Pd $3d_{3/2}$); 399.5 (N 1s, 4.8%); 531.5 (O 1s, 4.5%). ICP-AES: 3.33% Pd.

Synthesis of G2-PDI-Pd. The synthesis was carried out according to the procedure described above. The reactants included PAMAM-G2-PDI (300 mg) and $Pd(OAc)_2$ (64.8 mg, 0.288 mmol) in 30 mL of methylene chloride. The intermediate product was suspended in 30 mL of methylene chloride and 10 mL of methanol before adding sodium borohydride (109.87 mg, 2.88 mmol). The product was a black layered powder (70 mg).

IR (sm^{-1}): 3311 (N-H_{st} in NH-C(=O)); 2927 (C-H_{st}); 2856 (C-H_{st}, CH_2-N_{st}); 1631 (C=O_{st} in NH-C(=O)); 1549, 1510 (N-H_δ, $CH_{2\delta}$, C-N-H_δ); 1450, 1404 ($CH_{2\delta}$); 1298, 1221, 1107, 1016 (C-N_{st} in NH-C(=O)); 837, 823 (aromatic C-H_δ); 760, 648 (aromatic C=C_δ).

XPS (eV): 284.5 (46.28%), 285.5 (33.36%), 286.4 (9.04%), 288.4 (11.31%) (C 1s, 71.4%); 335.2 (50%) (Pd $3d_{5/2}$, 1.3%), 338.0 (50%) (Pd $3d_{3/2}$); 399.5 (N 1s, 16.4%); 531.1 (O 1s, 10.9%). ICP-AES: 4.61% Pd.

Synthesis of $G_2$2-PDI-Pd. The synthesis was carried out according to the procedure described above. The reactants included PAMAM-G2-PDI (500 mg), $Pd(OAc)_2$ (160 mg, 0.714 mmol) and sodium borohydride (271.2 mg, 7.14 mmol). The product was a black powder (94 mg).

IR (sm^{-1}): 3313 (N-H_{st} in NH-C(=O)); 2924 (C-H_{st}); 2534 (C-H_{st}, CH_2-N_{st}); 1631 (C=O_{st} in NH-C(=O)); 1556, 1510 (N-H_δ, $CH_{2\delta}$, C-N-H_δ); 1452, 1404 ($CH_{2\delta}$); 1298, 1221, 1109, 1014 (C-N_{st} in NH-C(=O)); 833, 821 (aromatic C-H_δ); 761, 640 (aromatic C=C_δ).

XPS (eV): 284.6 (53.94%), 285.6 (29.89%), 286.6 (6.72%), 288.4 (9.45) (C 1s, 75.9%); 335.0 (63%) (Pd $3d_{5/2}$, 1.4%), 338.0 (37%) (Pd $3d_{3/2}$); 399.5 (95.11%), 401.1 (4.89%) (N 1s, 13.5%); 531.1 (O 1s, 9.2%). ICP-AES: 6.23% Pd.

Synthesis of $G_3$2-PDI-Pd. The synthesis was carried out according to the procedure described above. The reactants included PAMAM-G2-PDI (604 mg), $Pd(OAc)_2$ (201 mg, 0.898 mmol) and sodium

borohydride (341.2 mg, 8.98 mmol) The product was a black layered powder (96 mg).

XPS (eV): 284.4 (44.95%), 285.5 (36.65%), 286.5 (6.93%), 288.5 (11.47%) (C 1s, 59.2%), 335.2 (51%) (Pd $3d_{5/2}$, 1.5%), 338.0 (49%) (Pd $3d_{3/2}$); 399.5 (N 1s, 26.7%); 531.0 (O 1s, 12.6%). ICP-AES: 6.8% Pd.

Synthesis of G2-DMPDI-Pd. The synthesis was carried out according to the procedure described above. The reactants included PAMAM-G2-DMPDI (743 mg) and $Pd(OAc)_2$ (0.386 g, 1.722 mmol) in 40 mL of absolute chloroform. The intermediate product was suspended in 30 mL of chloroform and 10 mL of methanol before adding sodium borohydride (0.654 g, 17.22 mmol). The product was a black powder (926 mg).

IR (sm^{-1}): 3305 (N-H_{st} in NH-C(=O)); 2933 (C-H_{st}); 2864 (C-H_{st}, CH_2-N_{st}); 1635, 1589 (C=O_{st} in NH-C(=O)); 1516 (N-H_δ, $CH_{2\delta}$, C-N-H_δ); 1454, 1392, 1321 ($CH_{2\delta}$); 1240, 1211, 1174, 1124, 1072, 1030 (C-N_{st} in NH-C(=O)); 853, 814, 796 (aromatic C-H_δ); 756, 648 (aromatic C=C_δ). XPS (eV): 284.3 (48.96%), 285.7 (42.65%), 288.2 (8.39%) (C 1s, 72.1%); 335.1 (38.88%) (Pd $3d_{5/2}$, 1.0%), 337.9 (61.12%) (Pd $3d_{3/2}$); 399.5 (N 1s, 13.5%); 530.9 (42.26%), 532.6 (57.74%) (O 1s, 13.4%); 532.7 (Pd $3p_{3/2}$). ICP-AES: 4.09% Pd.

Synthesis of G3-HMDI-Pd. The synthesis was carried out according to the procedure described above. The reactants included PAMAM-G3-HMDI (800 mg) and $Pd(OAc)_2$ (61.56 mg, 0.274 mmol) in 30 mL of methylene chloride. The intermediate product was suspended in 30 mL of methylene chloride and 10 mL of methanol before adding sodium borohydride (104.37 mg, 2.736 mmol). The product was a darkly coloured, resin-like polymer (530 mg).

IR (sm^{-1}): 3244 (N-H_{st} in NH-C(=O)); 2918 (C-H_{st}); 2860 (C-H_{st}, CH_2-N_{st}); 1630 (C=O_{st} in NH-C(=O)); 1547 (N-H_δ, $CH_{2\delta}$, C-N-H_δ); 1454, 1335 ($CH_{2\delta}$); 1254, 1190, 1132, 1070, 1020 (C-N_{st} in NH-C(=O)).

XPS (eV) 284.8 (52.5%), 285.8 (31.38%), 287.0 (4.87%), 288.1 (9.46%), 292.2 (1.8%) (C 1s, 74.2%); 338.2 (Pd $3d_{3/2}$; 0.3%); 399.5 (85.09%), 401.4 (14.91%) (N 1s, 14.7%); 531.2 (O 1s, 10.8%). ICP-AES: 1.66% Pd.

Synthesis of G3-PDI-Pd. The synthesis was carried out according to the procedure described above. The reactants included PAMAM-G3-PDI (800 mg) and $Pd(OAc)_2$ (246 mg, 1.096 mmol) in 30 mL of methylene chloride. The intermediate product was suspended in 30 mL of methylene chloride and 10 mL of methanol before adding sodium borohydride (416 mg, 10.944 mmol). The product was a darkly coloured, rubber-like polymer (357 mg).

IR (sm^{-1}): 3315 (N-H_{st} in NH-C(=O)); 2923 (C-H_{st}); 2844 (C-H_{st}, CH_2-N_{st}); 1633 (C=O_{st} in NH-C(=O)); 1547, 1508 (N-H_δ, $CH_{2\delta}$, C-N-H_δ); 1448, 1404 ($CH_{2\delta}$); 1298, 1241, 1211, 1182, 1107, 1043, 1011 (C-N_{st} in NH-C(=O)); 924, 862, 806 (aromatic C-H_δ); 756, 694, 671, 654 (aromatic C=C_δ).

XPS (eV): 284.3 (52.43%), 285.3 (26.50%), 286.2 (10.8%), 288.3 (10.28%) (C 1s, 60.7%) 335.1 (85%) (Pd $3d_{5/2}$, 1.6%), 338.0 (15%) (Pd $3d_{3/2}$); 399.5 (92.44%), 401.3 (7.56%) (N 1s, 21.9%); 531.6 (O 1s, 15.8%). ICP-AES: 13.73% Pd.

2.4. Catalytic test

A catalyst and a substrate (4 mg of the catalyst per 1 ml of substrate) were placed in a thermostated steel autoclave equipped with an insert test tube and a magnetic stirrer. If necessary, the solvent was added before sealing the autoclave tightly, filling it with 5–10 atm hydrogen, and connecting it to a thermostat. The reaction was performed with vigorous stirring at 80 °C for 15 min or 1 h; afterwards, the autoclave was cooled to below room temperature. The products were analysed using gas-liquid chromatography (GLC) on a ChromPack CP9001 gas chromatograph with a flame ionisation detector. The column was 30 m × 0.2 mm with an SE-30 grafted phase.

3. Results and discussion

3.1. Catalyst characterization

To prepare the networked polymer matrices used as supports for palladium nanoparticles, we used first-, second- and third-generation polyamidoamine (PAMAM) dendrimers ($PAMAM(NH_2)_8$), ($PAMAM(NH_2)_{16}$) and ($PAMAM(NH_2)_{32}$, respectively). The cross-linking agents were compounds that form conformationally labile links between dendrimers including 1,4-butylene diisocyanate - $OCN(CH_2)_4NCO$ (BDI), 1,6-hexamethylene diisocyanate - $OCN(CH_2)_6NCO$ (HMDI), 1,8-octamethylene diisocyanate - $OCN(CH_2)_8NCO$(OMDI), as well as compounds that form conformationally rigid links between the dendrimers (p-phenylene diisocyanate - $OCNC_6H_4NCO$ (PDI) and 3,3′-dimethoxy-4,4′-biphenylene diisocyanate–p-$(H_3COC_6H_3NCO)_2$ (DMPDI). The size, rigidity and polarity of the resulting cross-links were expected to affect the activity and selectivity of the catalysts. To compare the effects on the properties of the final hybrid material relative to the size of the cross-linker, materials based on $PAMAM(NH_2)_8$, $PAMAM(NH_2)_{16}$, $PAMAM(NH_2)_{32}$ with NCO/NH_2 ratios of 1:3 were synthesised (Table 1). The XPS data indicated that the process occurred through the traditional mechanism for the addition of an amine to an isocyanate to form–NH-C(=O)-NH–fragments (Scheme 1).

Metal nanoparticles were encapsulated in dendrimers according to the procedure described in [24]: complexation with a transition metal salt followed by a reduction with sodium borohydride (Scheme 2). The polymer matrices were based on dendrimers cross-linked with diisocyanates; these materials were used to prepare the palladium catalysts. The metal deposition step was carried out in chloroform due to good solubility of palladium acetate and the swelling ability exhibited by this solvent with polymers containing urethane groups. The reduction to Pd(0) was achieved using sodium borohydride.

The amount of metal deposited on the polymer depended on the dendrimeric structure, as well as the nature and density of the cross linker. The metal content (in %) for each of the prepared materials was determined by ICP-AES, as listed in Table 1.

3.2. X-ray photoelectron spectroscopy (XPS) study

The obtained materials were characterised using XPS technique. The XPS data are presented in Table 1. Palladium atoms in two distinct states were observed for the G1-BDI-Pd, G1-HMDI-Pd, G1-OMDI-Pd, G1-PDI-Pd and G1-DMPDI-Pd samples. The binding energies for Pd $3d_{5/2}$ were 335.7 eV and 335.2 eV for the HMDI and PDI cross-linking agents and for the BDI, OMDI and DMPDI cross-linking agents, respectively. It can be attributed to the metallic palladium. The binding energies for the HMDI and PDI cross-linking agents and the BDI, OMDI, and DMPDI cross-linking agents were 338.2 eV and 337.9 eV, respectively. The line for this binding energy was closer to that of palladium oxide (according to the energy position and shift relative to the value of metallic palladium). In the G2-HMDI-Pd and G3-HMDI-Pd samples, one state of palladium atoms was observed: Pd^{+2}. However, the Pd content was twice as high in G_22-HMDI-Pd as in G2-HMDI-Pd. In G_22-HMDI-Pd, two shifts that indicate two oxidation states of palladium (Pd^0 and Pd^{+2}) were apparent. In G1-PDI-Pd, G2-PDI-Pd, G_22-PDI-Pd, G_32-PDI-Pd and G3-PDI-Pd, as shown in Table 1, two oxidation states were observed for palladium. Therefore, while using the PDI cross-linking agent to synthesise the catalyst, the dendrimer generation and the Pd content do not influence the state of the palladium; the same is true when using the HMDI cross-linking agent.

The binding energies for Pd $3d_{5/2}$ and Pd $3d_{3/2}$ are 335.7 eV and 338.2 eV, respectively, i.e., they are slightly lower than that

Table 1
Catalysts and their characterisation data.

Dendrimer	Cross-linking agent	Indication of a catalyst	Pd (%)	Pd $3d_{5/2}$ (эВ)	Pd $3d_{3/2}$ (eV)	Surface atomic concentration (%)	Particle size, *d* (nm)
PAMAM$(NH_2)_8$	OCN$(CH_2)_4$NCO	G1-BDI-Pd	15.83	335.0 (87%)	337.9 (13%)	4.7	1.47 ± 0.08; 2.7 ± 0.24
PAMAM$(NH_2)_8$	OCN$(CH_2)_6$NCO	G1-HMDI-Pd	14.8	335.7 (62%)	338.2 (38%)	8.9	2.1 ± 0.44
PAMAM$(NH_2)_8$	OCN$(CH_2)_8$NCO	G1-OMDI-Pd	5.45	335.2 (68%)	338.0 (32%)	1.2	1.84 ± 0.13
PAMAM$(NH_2)_8$	OCNC_6H_4NCO	G1-PDI-Pd	6.5	335.7 (45%)	338.2 (55%)	3.9	2.49 ± 0.25
PAMAM$(NH_2)_8$	*p*-$(H_3COC_6H_3NCO)_2$	G1-DMPDI-Pd	13.12	335.2 (83%)	337.9 (17%)	6.5	2.29 ± 0.1; 3.83 ± 0.22
PAMAM$(NH_2)_{16}$	OCN$(CH_2)_6$NCO	G2-HMDI-Pd	1.61		338.5 100%)	0.3	1.74 ± 0.05; 3.55 ± 0.24
PAMAM$(NH_2)_{16}$	OCNC_6H_4NCO	G2-PDI-Pd	4.61	335.2 (50%)	338.0 (50%)	1.3	1.07 ± 0.02; 1.46 ± 0.09
PAMAM$(NH_2)_{16}$	OCN$(CH_2)_6$NCO	$G_2$2-HMDI-Pd	3.33	334.8 (50%)	337.9 (50%)	0.3	2.01 ± 0.08; 3.13 ± 0.15
PAMAM$(NH_2)_{16}$	OCNC_6H_4NCO	$G_2$2-PDI-Pd	6.23	335.0 (63%)	338.0 (37%)	1.4	1.09 ± 0.12; 1.89 ± 0.12
PAMAM$(NH_2)_{16}$	OCNC_6H_4NCO	$G_3$2-PDI-Pd	6.8	335.2 (51%)	338.0 (49%)	1.5	
PAMAM$(NH_2)_{16}$	*p*-$(H_3COC_6H_3NCO)_2$	G2-DMPDI-Pd	4.09	335.1 (39%)	337.9 (61%)	1.0	2.22 ± 0.11
PAMAM$(NH_2)_{32}$	OCN$(CH_2)_6$NCO	G3-HMDI-Pd	1.66		338.2 100%)	0.3	1.92 ± 0.49
PAMAM$(NH_2)_{32}$	OCNC_6H_4NCO	G3-PDI-Pd	13.73	335.1 (85%)	338.0 (15%)	1.6	1.55 ± 0.03;2.25 ± 0.03

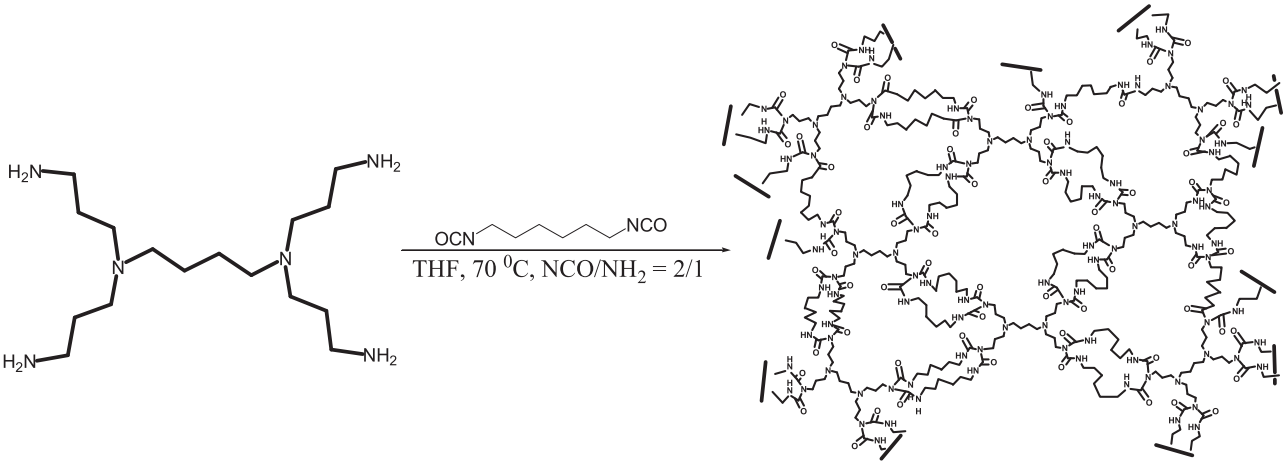

Scheme 1. Synthesis of polymeric materials based on cross-linked dendrimers.

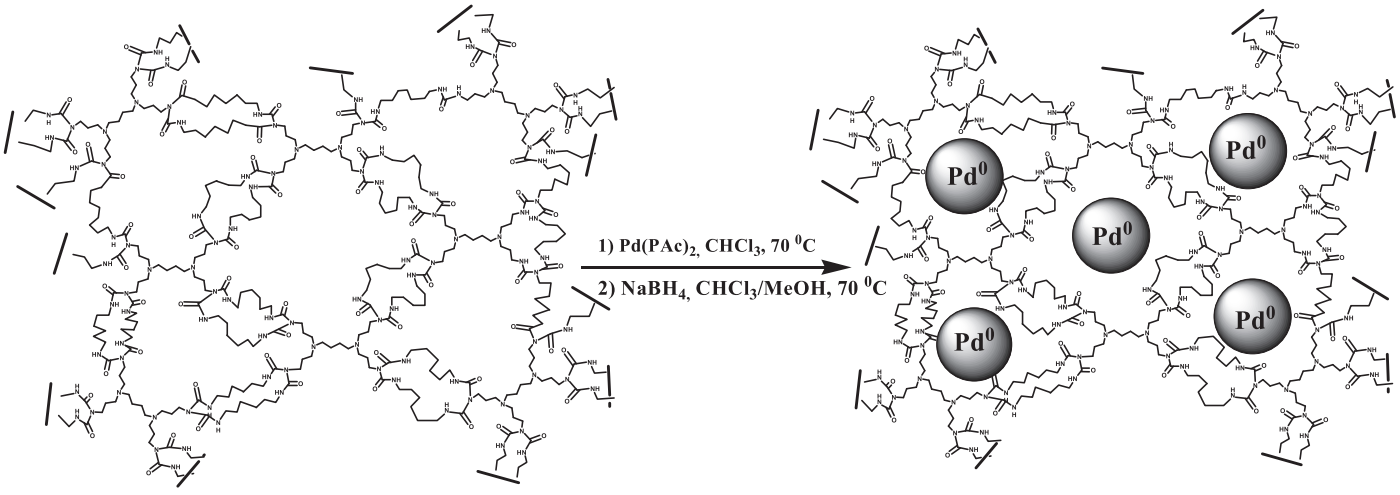

Scheme 2. Encapsulation of the palladium nanoparticles in cross-linked dendrimers.

of metallic palladium (0) (Pd: 335.8 eV [25]) and a little bit higher than that of divalent palladium (PdO: 337.9 [25]) The presence of these species was confirmed by the presence of metal nanoparticles coordinated by nitrogen or oxygen atoms. According to the component ratios in the Pd 3d electron spectrum (%), the ratios of the palladium metal (Pd^0) to the oxidised palladium (Pd^{2+}) on the sample surface are as follows:

- 87:13 for G1-BDI-Pd, 62:38 for G1-HMDI-Pd, 68:32 for G1-OMDI-Pd, 45:55 for G1-PDI-Pd, 83:17 for G1-DMPDI-Pd;
- 0:100 for G2-HMDI-Pd, 50:50 for G2-PDI-Pd, 50:50 for $G_2$2-HMDI-Pd, 63:37 for $G_2$2-PDI-Pd, 51:49 for $G_3$2-PDI-Pd;
- 0:100 for G3-HMDI-Pd and 85:15 for the G3-PDI-Pd.

The XPS data confirmed the presence of the C, N and O atoms, as well as entities such as $CH_2CH_2C(O)NH$ (the binding energies for O and N are 531.5 eV and 399.6 eV, respectively [25]), CH_2CH_2 (the C binding energy is 284.9 eV [25]), $CH_2CH_2NH_2$ (the C binding energy is 285.5 eV [25]), (CH_2NH_2)Pd (the C binding energy is 286.8 eV [25]) and $CH_2CH_2C(O)NH$ (the C binding energy is 288.1 eV [25]). The

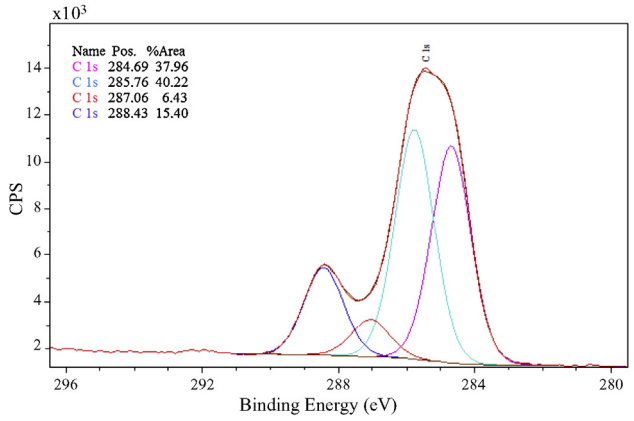

Fig. 1. C 1s-spectrum for G1-BDI-Pd.

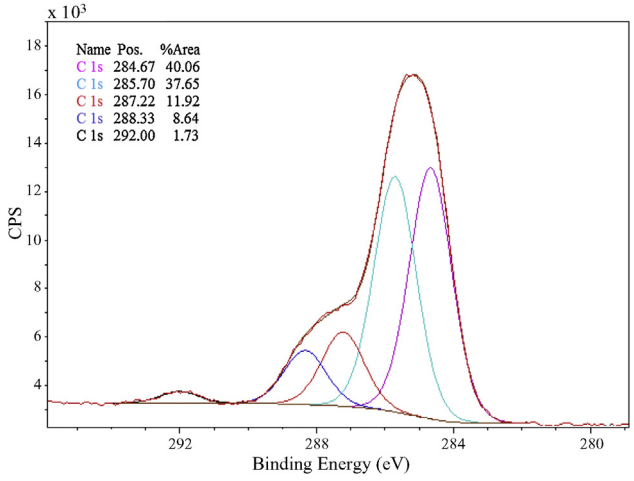

Fig. 2. C 1s-spectrum for G1-OMDI-Pd.

energy shift for oxygen and nitrogen relative to the normal values (531.5 eV and 398.6 eV, respectively [25]) in the spectra for the samples is due to a partial transfer of electrons to the neutral metal particles. In the G2-PDI-Pd (2) and G3-PDI-Pd samples, the binding energy of N is 401.3 eV, confirming the presence of C_6H_5NH and indicating that the cross-linking agent is p-phenylene diisocyanate.

The carbon deconvolution spectra show that the bond energies are approximately the same; however, the bond energies of C-C, C-N, C-Pd and C-O differ significantly. While considering the binding energies of samples with conformationally labile cross-linkers such as BDI, HMDI, and OMDI, the intensity of the C-C bonds (from 37.96% to 53.20%) increases, and the intensity of the C-N bonds decreases (from 40.22% up to 30.34%) when increasing the chain length. The highest intensity for the C-Pd bond (11.92%) is observed in the sample containing the hexamethylene diisocyanate cross-linker, while the lowest is observed in the sample with octamethylene diisocyanate cross-linker (4.82%); the intensity of this bond is not affected by the palladium content.

The C 1s-spectra for the G1-BDI-Pd (Fig. 1) and G1-OMDI-Pd (Fig. 2) are almost identical. There are two signals of 288.4 eV and 285.2 eV, which correspond to the energies of the C-O bond and the C–C and C–N bonds, respectively. The carbonyl bond, C-O, formed through the interactions of the amino groups on the dendrimer and the cross-linker, is present in the dendrimer and the periphery. The intensity ratio for the C-O and C-N bonds is the same in all of the samples (0.38:1). Similarly, the analogous proportion for $NCO/NH_2 = 1/2.6$.

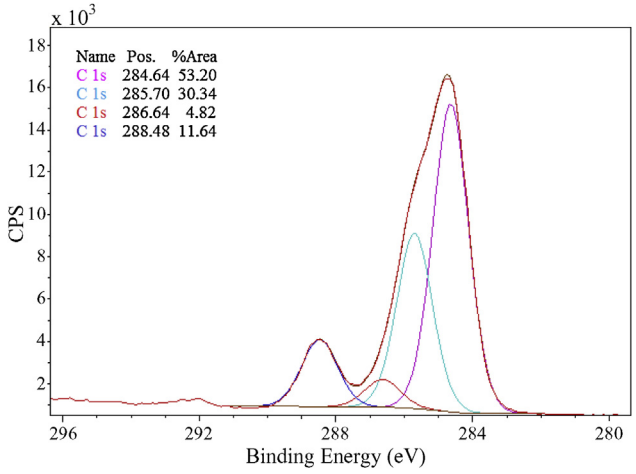

Fig. 3. C 1s-spectrum for the G1-HMDI-Pd.

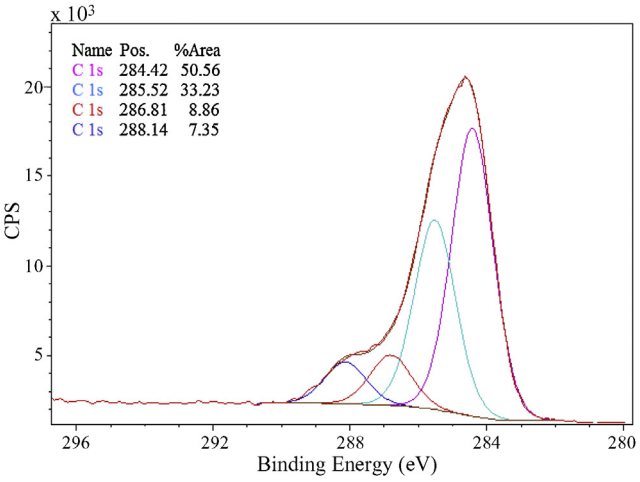

Fig. 4. C 1s-spectrum for G1-PDI-Pd.

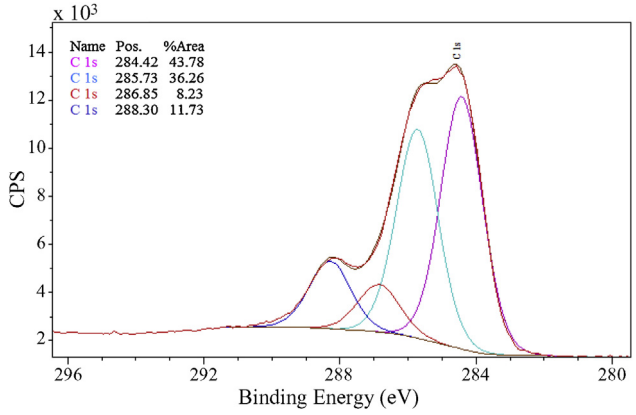

Fig. 5. C 1s-spectrum for G1-DMPDI-Pd.

In addition, the deconvolution graphs for G1-HMDI-Pd (Fig. 3) and G1-PDI-Pd (Fig. 4) have almost the same shape. Similarly, we can calculate the NCO/NH_2 ratio for these samples: 1/4.3. The NCO/NH_2 ratio is 1/3 in the G1-DMPDI-Pd sample (Fig. 5).

The intensities of the C and Pd bond are almost identical in the samples with rigid cross-linkers; the percentage and surface atomic concentration of palladium is approximately twice as high in the sample of G1-DMPDI-Pd as in G1-PDI-Pd.

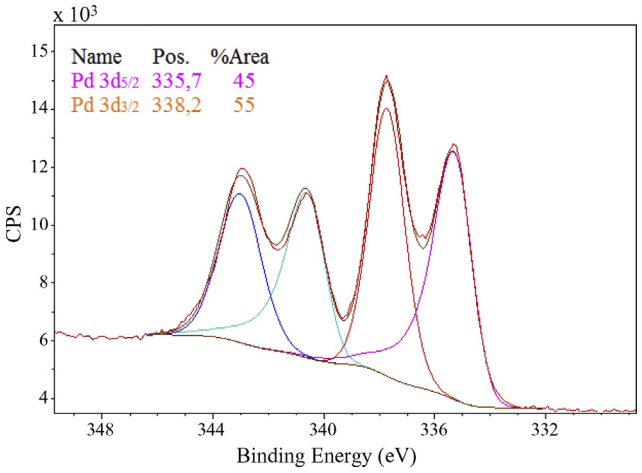

Fig. 6. Pd 3d-electron spectrum for G1-BDI-Pd.

The ratio of atomic concentrations of Pd (II)/Pd (0) is ~1.22 in the G1-BDI-Pd sample, as shown in Fig. 6, according to the deconvolution spectrum.

3.3. TEM analysis

Based on the TEM data, the size and shape of the distributions are affected by the cross-linker and dendrimer generation for composites based on palladium nanoparticles (Figs. 7–18).

The monomodal and bimodal particle size distributions are obtained based on the first generation of the PAMAM dendrimer while using four different cross-linkers. The distribution is affected by the chain length of the cross-linker. While using hexamethylene diisocyanate, a monomodal distribution is observed (Fig. 8), but while using butylene diisocyanate, a bimodal distribution (1.5 and 2.7 nm, Fig. 7) is observed. This difference might be associated with the size of the cavities in the dendritic structure. While using this cross-linker, two adjacent branches of the dendrimer bound due to the short carbon chain of the cross-linker. Therefore, the cavities for smaller particles of 1.4–1.6 nm are formed and stabilised by the tertiary nitrogen atoms.

In addition, the pattern of the dendrimer generation exerts a visible influence. While using hexamethylene diisocyanate, a monomodal distribution is observed with maxima of 2.1 and 1.9 nm for the samples obtained based on the first and third generations, respectively (Figs. 8 and 17). For a sample obtained based on the second generation, a bimodal distribution is observed with maxima at 1.7 and 3.6 nm (Figs. 12 and 14). The distribution of the samples obtained using another cross-linker, namely p-phenylene diisocyanate, is similar. There is a monomodal distribution in the sample based on the first generation (Fig. 10), while a bimodal distribution is observed in the sample based on the second (Figs. 13 and 15) and the third generations (Fig. 18). Increasing the generation leads to a bimodal distribution; the 1.5–2-nm particles might be located between the branches, while the 2.5–3-nm particles are situated in cavities.

The palladium content does not affect the particle distribution in the G2-HMDI-Pd and $G_2$2-HMDI-Pd catalysts, as shown in Figs. 6 and 8. A similar situation is observed for the G2-PDI-Pd and $G_2$2-PDI-Pd samples (Figs. 7 and 9). Increasing the palladium content increases the particle sizes: 1.7 and 2.3 for 1.66% Pd and 2.1 and 3.2 for 3.33% Pd in the G2-HMDI-Pd and $G_2$2-HMDI-Pd samples, respectively (Figs. 12 and 14). Similarly, while using another cross-linker (p-phenylene diisocyanate) the particle sizes are as follows: 1.0 and 1.6 nm are for 4.61% Pd, and 1.2 and 1.9 nm are for 6.23% Pd for the G2-PDI-Pd and $G_2$2-PDI-Pd samples (Figs. 13 and 15).

Using a harder cross-linker (p-phenylene diisocyanate) relative to hexamethylene diisocyanate increases the cavity size and, consequently, the particle size: 2.5 and 2.1 nm for G1-PDI-Pd and G1-HMDI-Pd, respectively (Figs. 10 and 8).

When using a more rigid cross-linker (3,3′-dimethoxy-4,4′-diphenylene diisocyanate), larger particles (2.3–2.5 and 3.8–4.0 nm, Fig. 11; 2.0–2.3 nm, Fig. 16) form due to the π-interactions, which retain the palladium particles through the additional phenyl ring.

3.4. Solid state NMR spectroscopy

The carbon polarisation transfer spectra (^{13}C CPMAS) were recorded to determine the local structure of the compounds. The spectra of the G1 series are as follows (Fig. 19).

Some areas of the signals were observed for the G1-BDI-Pd sample. In the region from 15 to 45 ppm, the carbon atoms on the methylene units of the initial dendrimer and the cross-linking agent (BDI) absorb. In addition, the weaker the field of the signal (closer to 50 ppm), the closer is the carbon atom to the nitrogen atom. The carbon signals for in the CH_2NH_2 groups have the highest intensity. The broader profile of the signals reveals the low regularity of the dendrimer groups in the structure. The signal at approximately 160 ppm appears to be the carbon in the –NH–(C═O)–NH– group formed during cross-linking. The broad low-intensity signal at 172 ppm might correspond to an unreacted isocyanate group (–N═C═O). The low-intensity signals at 83 and 115 ppm are likely impurities.

Two intense signals at 33 ppm and approximately 40.5 ppm are observed in the spectrum for the G1-HMDI-Pd sample. The first signal corresponds to the carbon in the $–CH_2$ groups β to the amino groups, while the second corresponds to an α position carbon to the $–NH_2$ groups. The $–N(CH_2)_3$ signal is the low-intensity shoulder at approximately 55 ppm. The low-intensity signal at approximately 160 ppm corresponds to the –NH–(C═O)–NH– group.

The spectrum of the G1-OMDI-Pd sample is similar to that of the G1-HMDI-Pd; two signals are observed in the aliphatic region of the dendrimer, and one low-intensity signal corresponds to the carbide carbon.

An intense signal at approximately 40 ppm ($–CH_2NH_2$ group) spanning from 20 to 50 ppm is observed for the G1-PDI-Pd sample. The $–N(CH_2)_3$ groups are in the shoulder at approximately 55 ppm. The signals from 120 to 135 ppm correspond to the carbon centre of the benzene ring; the lowest field signal (at 133.2 ppm) is the carbon linked to the –NH–(C═O)–NH– group. The signal at approximately 160 ppm corresponds to the carbonyl carbon. The spectra show that the G1-PDI-Pd and G1-PDI samples are identical without palladium nanoparticles.

For the G1-DMPDI-Pd sample from 20 to 60 ppm, the two narrow intense signals (40.6 and 55.3 ppm) correspond to the $–CH_2NH_2$ and $–N(CH_2)_3$ groups. Notably, the signal at approximately 55 ppm in other samples was less intense. This effect might be caused by the insertion of the Pd nanoparticles, which favours the carbon centre patterning due to their coordination. Therefore, for cross-linked dendrimers, the type of cross-linking agent might favour the conditions necessary for Pd nanoparticle coordination in all dendrimer nitrogen centres due to its bulk and rigidity. In addition, the –OMe groups bound to the benzene ring absorb at 55 ppm. The group of signals between 105 and 160 ppm corresponds to the carbon centres of the benzene ring, with the lowest field signal (the carbon bound to the OMe group) at approximately 160 ppm overlapping with the –NH–(C═O)–NH– signal.

The spectra of the G2 series (the samples based on the second-generation dendrimer) are shown in Fig. 20.

The interpretation of these spectra is analogous to that of the G1 series (the samples synthesised based on the second-generation

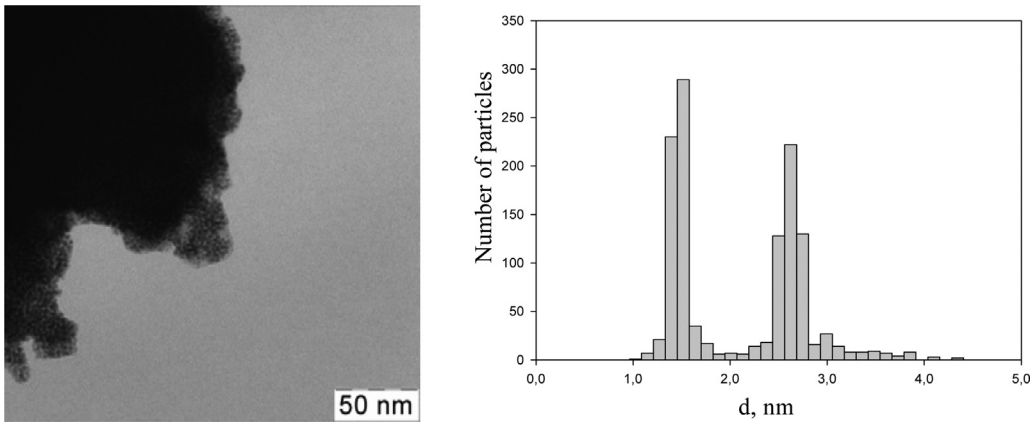

Fig. 7. TEM data and particle size distribution for G1-BDI-Pd.

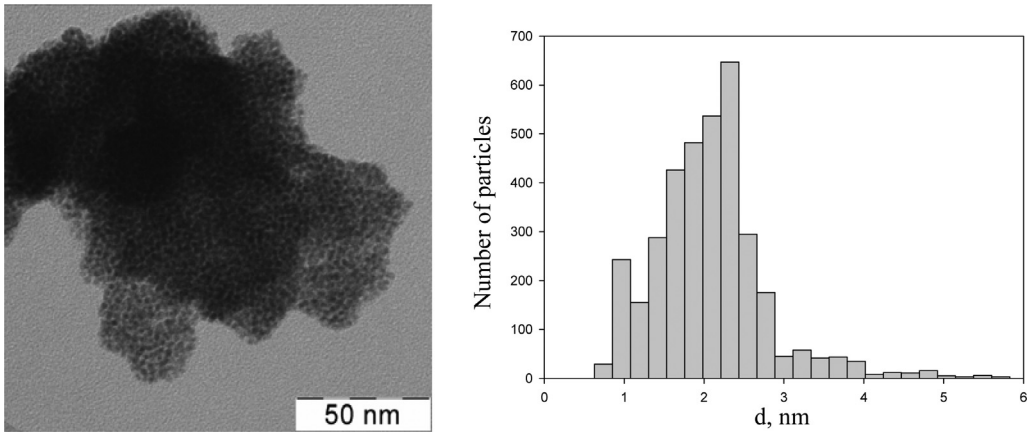

Fig. 8. TEM data and particle size distribution for G1-HMDI-Pd.

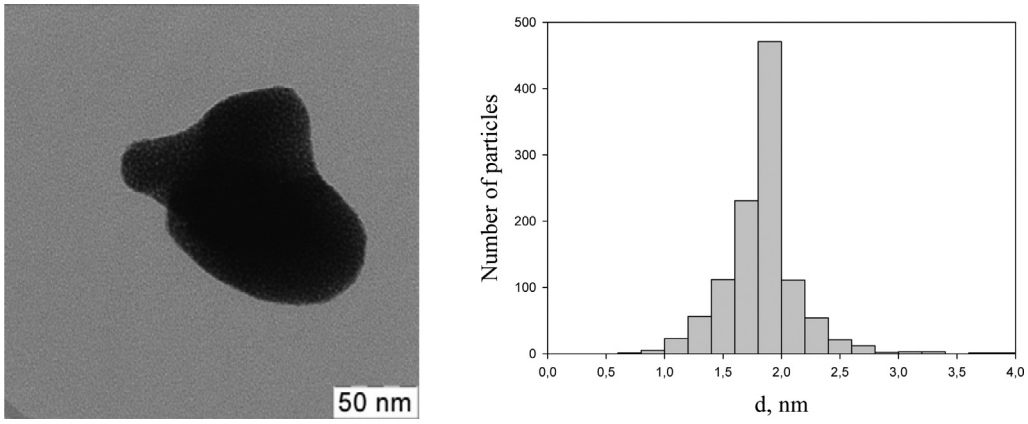

Fig. 9. TEM data and particle size distribution for G1-OMDI-Pd.

dendrimers). Therefore, only the very weak signal attributed to the –NH–(C═O)–NH– group is notable for the samples with the HMDI cross-linking agent in contrast to the sample with the PDI cross-linking agent. This weakness in the signal might occur because the carbide carbonyl is labile and/or the cross-linker content is low.

When comparing the spectra of the G2-PDI-Pd and $G_2$2-PDI-Pd samples, the signals assigned to the dendrimer are different. G2-PDI-Pd has only one intense signal at approximately 44 ppm in contrast to $G_2$2-PDI-Pd. This difference might be due to the differing amounts of palladium in the dendrimer. The palladium nanoparticles in G2-PDI-Pd might coordinate with the $-(CH_2)_3N$ centres, leaving the $-CH_2NH_2$ centre free and imparting a lability higher than the original dendrimer; therefore, the polarisation transfer to these centres is low over a given contact time. The CH_2NH_2 sample centres are locked in the $G_2$2-PDI-Pd structure, leaving them visible.

The spectra for the samples with the HMDI cross-linking agent, including the G3-HMDI-Pd sample, are shown below in Fig. 21. The spectra are almost identical, except that the signal at approximately 51 ppm for G3-HMDI-Pd is the most intense.

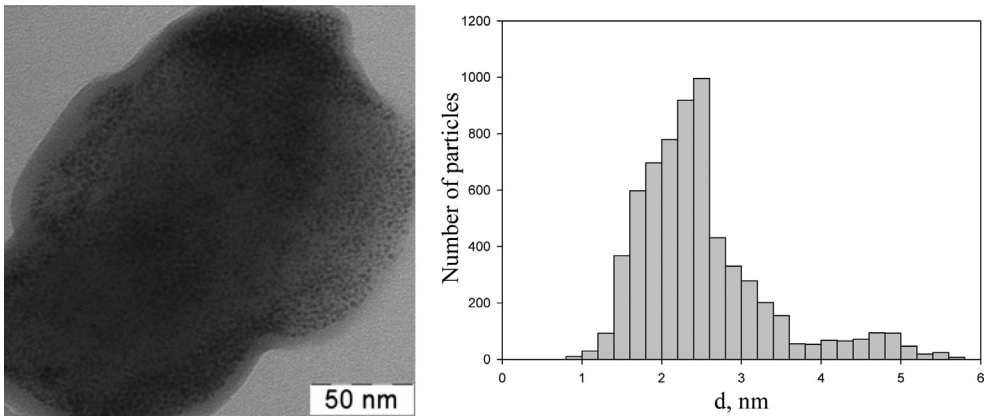

Fig. 10. TEM data and particle size distribution for G1-PDI-Pd.

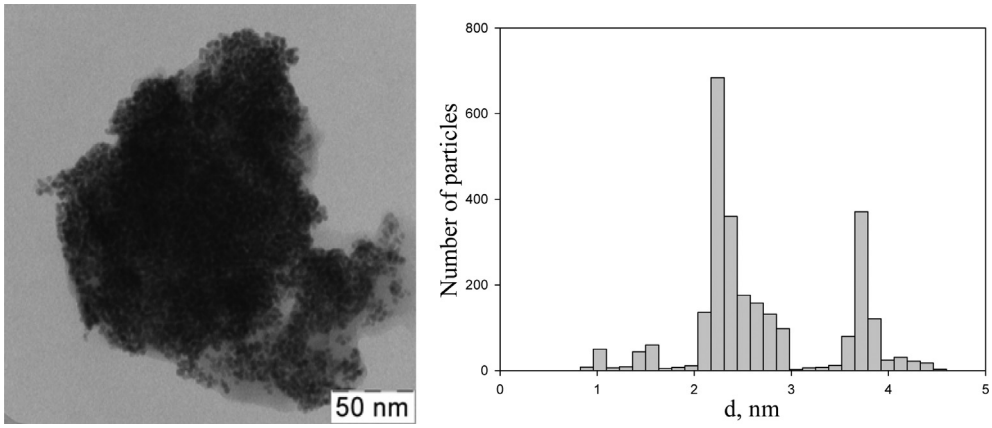

Fig. 11. TEM data and particle size distribution for G1-DMPDI-Pd.

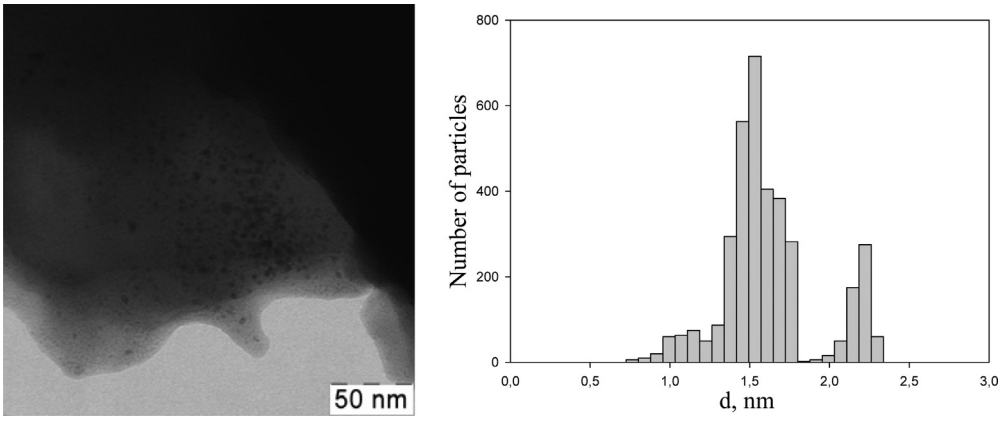

Fig. 12. TEM data and particle size distribution for G2-HMDI-Pd.

3.5. Hydrogenation of unsaturated compounds

3.5.1. Hydrogenation of octene-1

The synthesised materials were tested as hydrogenation catalysts for unsaturated compounds. When a terminal linear olefin, such as octene-1, was hydrogenated in the presence of the synthesised materials (Fig. 22), the maximum conversions were achieved using G1-HMDI-Pd and $G_2$2-PDI-Pd: 83% and 78%, respectively. When using catalysts based on the first-, second- and third-generation PAMAM dendrimers with the HMDI cross-linker, the yields increase in the following order: G3-HMDI-Pd < G2-HMDI-Pd « $G_2$2-HMDI-Pd < G1-HMDI-Pd (Fig. 22a). This trend corresponds to the increase in palladium content, and the dendrimer generation does not affect the conversion.

When using catalysts based on the first- and second-generation PAMAM dendrimers with the PDI cross-linker, the yields increase in the following order: G2-PDI-Pd « G1-PDI-Pd < $G_2$2-PDI-Pd (Fig. 22b). Moreover, the palladium content is nearly equal in the G1-PDI-Pd and $G_2$2-PDI-Pd samples, but the conversion is approximately 10% higher for $G_2$2-PDI-Pd, possibly due to the size of the palladium particles. The particle size in the first sample is twice that of the second.

When using catalysts based on the first generation of dendrimers and various cross-linkers, another relationship is observed

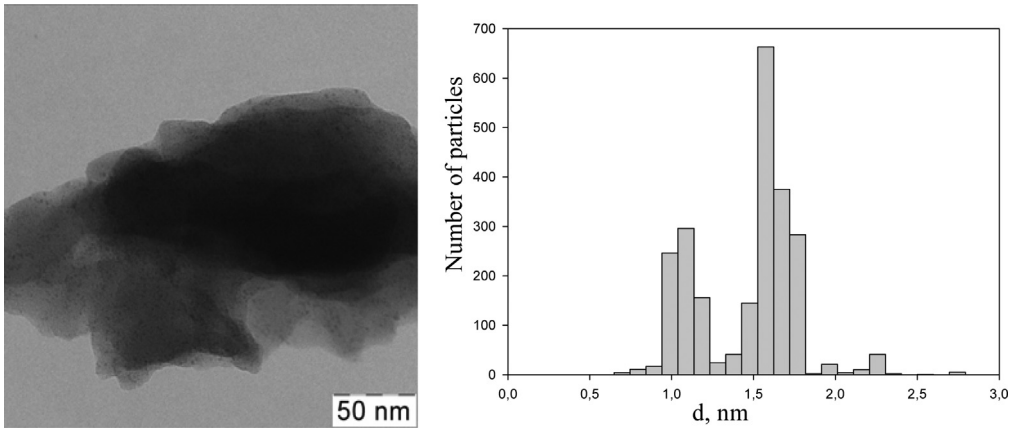

Fig. 13. TEM data and particle size distribution for G2-PDI-Pd.

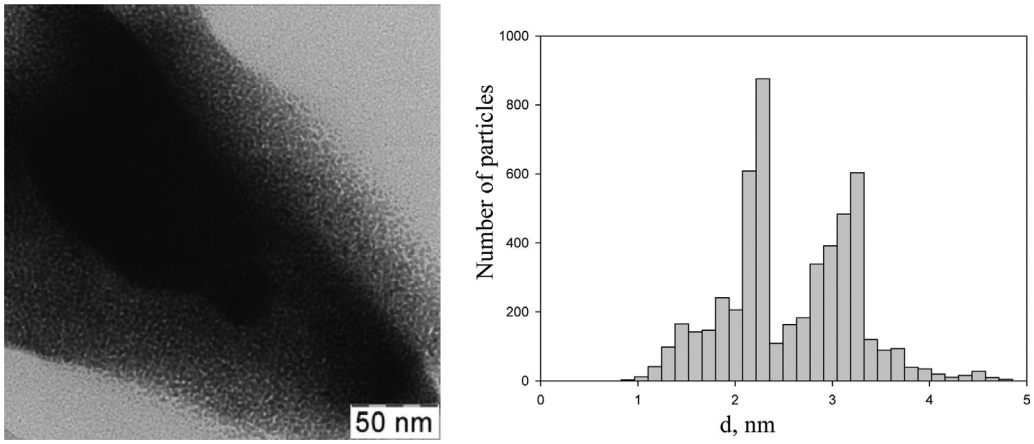

Fig. 14. TEM data and particle size distribution for $G_2$2-HMDI-Pd.

(Fig. 22c). The yields increase in the following order: G1-OMDI-Pd < G1-BDI-Pd < G1-PDI-Pd < G1-DMPDI-Pd < G1-HMDI-Pd. In this case, the conversion does not depend on the palladium content because the yields are almost identical when using G1-BDI-Pd (15.83%) and G1-PDI-Pd (6.5%), namely 63% and 69%, respectively. Based on this graph, the conversion is affected by the cross-linker. A low conversion can be explained by steric hindrance during the substrate coordination when using conformationally rigid cross-linkers such as para-phenylene diisocyanate and 3,3′-dimethoxy-4,4′-biphenylene diisocyanate and "short" cross-linkers such as 1,4-butylene diisocyanate.

Graphs describing the activity toward octene hydrogenation are shown in Fig. 23. When using catalysts based on the PAMAM dendrimers of various generations with the HMDI linker, the $G_2$2-HMDI-Pd sample exhibits highest activity (TOF = $13.6 \times 10^3\ h^{-1}$) (Fig. 23a).

For similar catalysts with the PDI cross-linking agent, the maximal value of TOF of $8.5 \times 10^3\ h^{-1}$ is observed in the $G_2$2-PDI-Pd

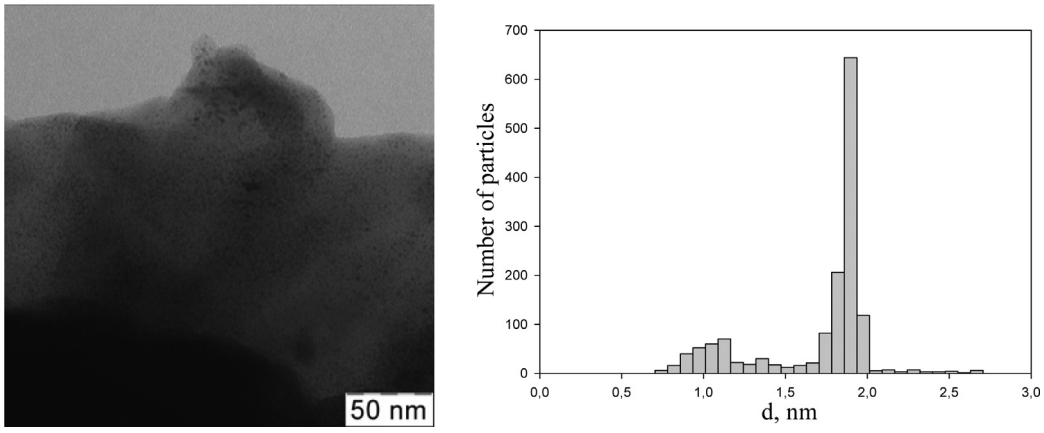

Fig. 15. TEM data and particle size distribution for $G_2$2-PDI-Pd.

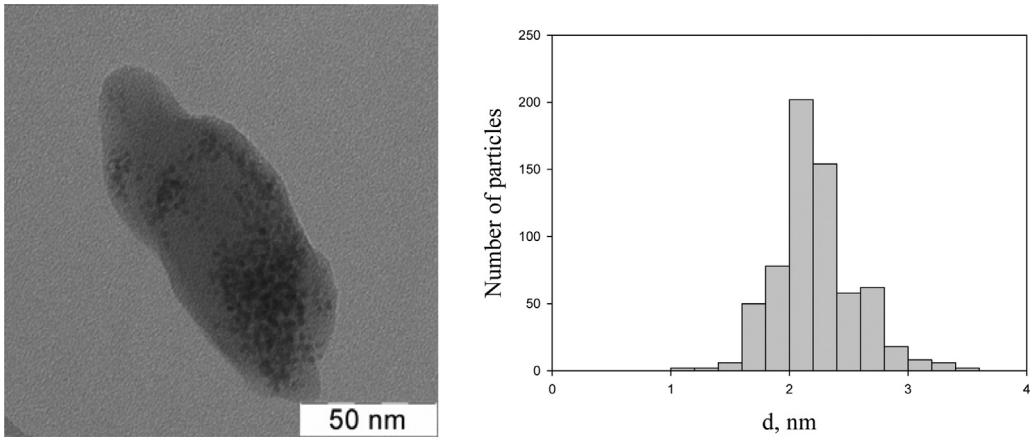

Fig. 16. TEM data and particle size distribution for G2-DMPDI-Pd.

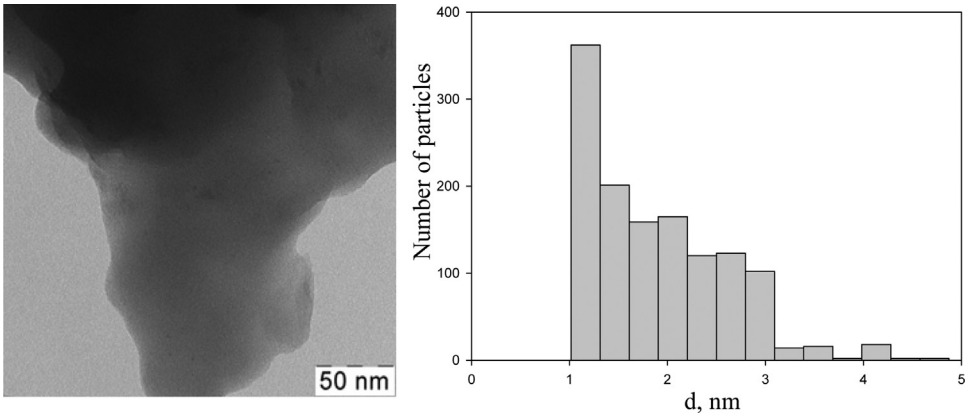

Fig. 17. TEM data and particle size distribution for G3-HMDI-Pd.

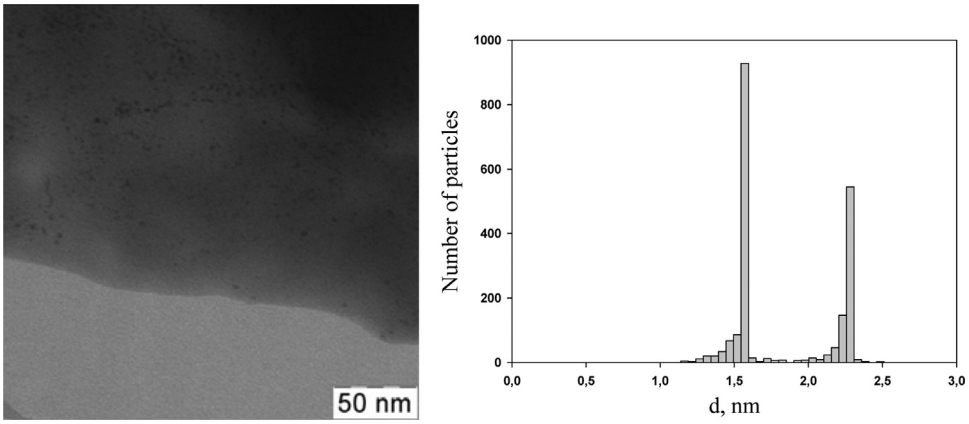

Fig. 18. TEM data and particle size distribution for G3-PDI-Pd.

sample (Fig. 23b); this value is less than that while using the HMDI cross-linker.

The variations in the octene hydrogenation when using the first-generation PAMAM dendrimer with various cross-linking agents are shown in Fig. 23 (graph c). The catalytic activity decreased in the following order due to the increasing steric hindrance during substrate coordination: G1-PDI-Pd » G1-DMPDI-Pd > G1-HMDI-Pd > G1-OMDI-Pd > G1-BDI-Pd.

Simultaneously, the proportion of the double bond isomerisation product increases in the reaction mixture; the higher the proportion, the longer is the chain. The isomerism of double bonds in the presence of palladium is quite facile (Scheme 3), generating internal alkenes that are more thermodynamically stable internal alkenes. The latter product is more sterically hindered than terminal alkenes, preventing the substrate from taking the conformation necessary for the reaction with the available ligand microenvironment; therefore, these substrates are hydrogenated with low yields.

3.5.2. Hydrogenation of styrene, p-methylstyrene and p-tert-butylstyrene

Materials based on palladium nanoparticles and cross-linked dendrimers were highly active during the hydrogenation of

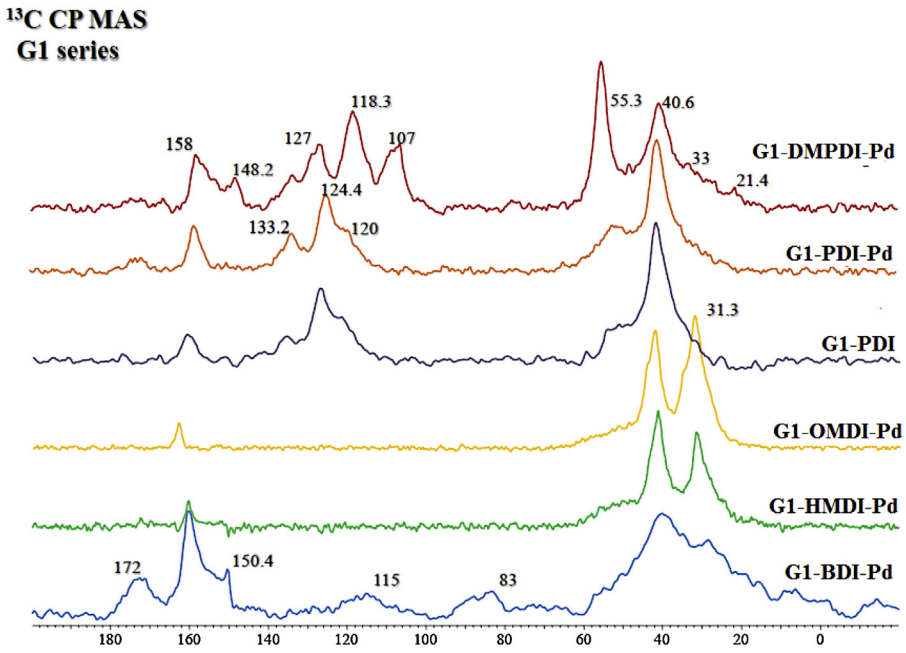

Fig. 19. ^{13}C CP MAS spectra for the samples synthesised based on the first generation PAMAM dendrimer with various cross-linking agents.

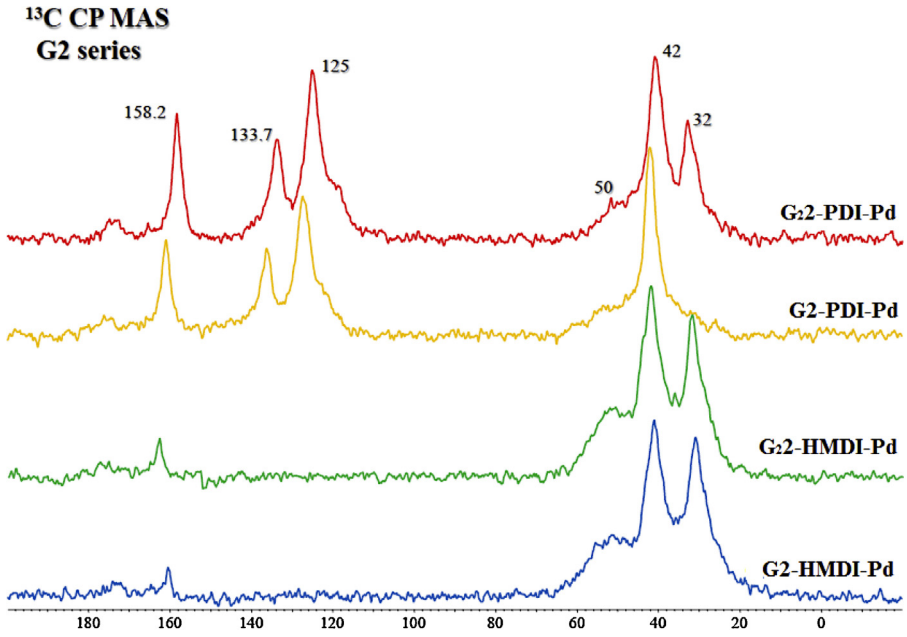

Fig. 20. ^{13}C CP MAS spectra for the samples synthesised based on the second-generation PAMAM dendrimer.

styrene and its derivatives, forming the corresponding ethylbenzene (Figs. 24–26, Scheme 4), with a TOF value close to 86×10^3 h^{-1}, which is significantly higher than that for 1-octene.

The best catalyst for the hydrogenation of styrene and p-tert-butylstyrene is G1-PDI-Pd; 100% conversion was achieved in all of the reactions using this catalyst (Fig. 25a).

The effect of the PAMAM dendrimer generation with the 1,6-hexamethyldiisocyanate linker on the conversion and hydrogenation activity of styrene is shown in Fig. 24. The highest conversion is observed with the G1-HMDI-Pd catalyst; the conversion also increases when increasing the size of the substrate (Fig. 24a). Therefore, the conversion is affected by the palladium content rather than the dendrimer generation. The worst catalyst for the hydrogenation of styrene and its derivatives is G3-HMDI-Pd, which has the lowest palladium content. The G3-HMDI-Pd catalyst is the most active during the styrene hydrogenation; its TOF is 35.2×10^3 h^{-1} (Fig. 24b).

In this case, the yields depended on the size of the substrate. Therefore, for G1-HMDI-Pd, regular increases in activity were observed when increasing the size of the substrate; this catalyst is not affected by steric hindrance. However, the G1-BDI-Pd, G1-OMDI-Pd, $G_2$2-HMDI-Pd, G3-HMDI-Pd and G3-PDI-Pd catalysts exhibited a parabolic dependence on the size of the substrate for the activity; a minimum for p-methylstyrene and maximum for styrene were characteristic (Figs. 26a and 24a).

For these materials, the substrate has an optimal size corresponding to the distance between the branches of the dendritic matrix. For the G1-DMPDI-Pd, G2-PDI-Pd, $G_2$2-PDI-Pd and

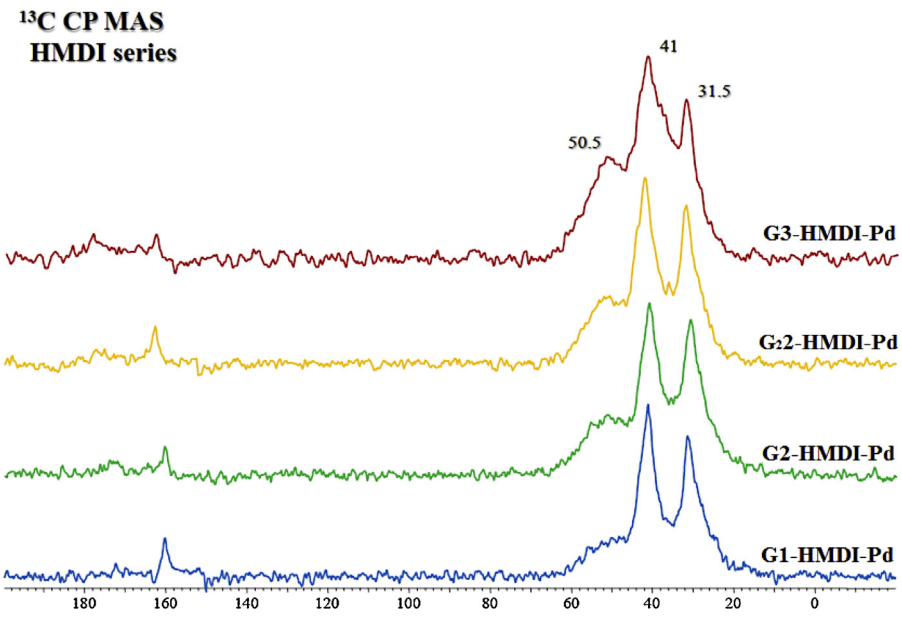

Fig. 21. ^{13}C CP MAS spectra for the samples synthesised based on the first-, second- and third-generation PAMAM dendrimers with the HMDI cross-linker.

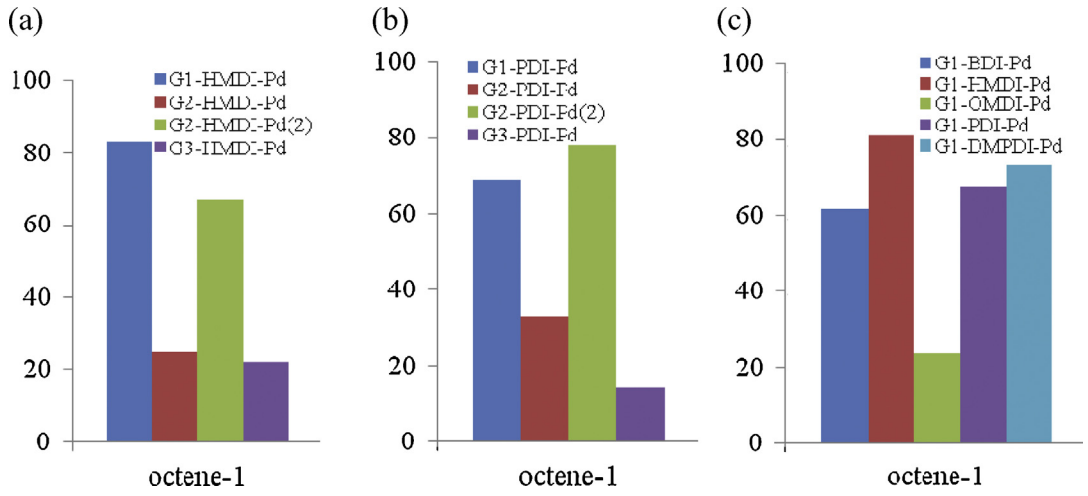

Fig. 22. The relationship between dendrimer generation and the conversion of the cross-linked palladium catalysts (HMDI (a) and PDI (b)) and the effect of the cross-linking agent (c). Reaction conditions: 4 mg of the catalyst per 1 mL of the substrate, 80 °C, 1 h, 10 atm H_2.

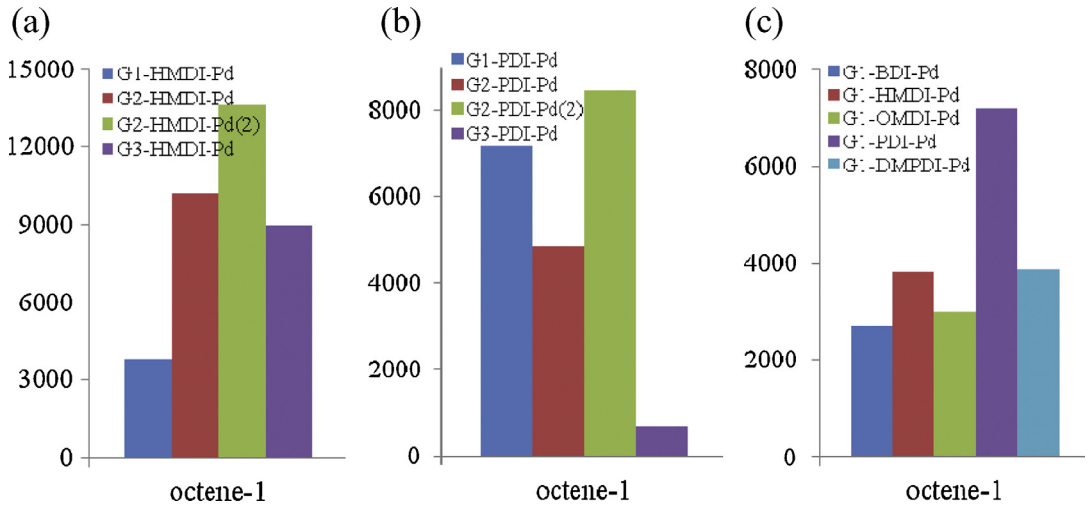

Fig. 23. The effect of dendrimer generation on the hydrogenation activity for palladium catalysts with the HMDI (a) and PDI cross-linkers (b), as well as the effect of the cross-linking agent (c). Reaction conditions: 2 mg of the catalyst per 1 mL of the substrate, 80 °C, 1 h, 10 atm H_2.

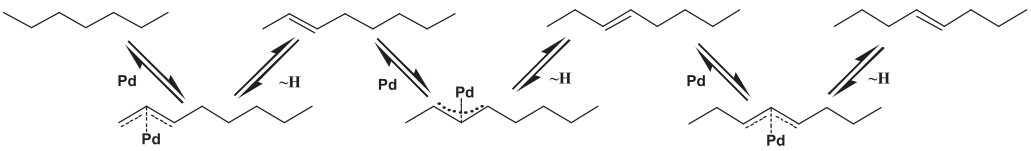

Scheme 3. Isomerisation of the double bond, as exemplified by octene-1.

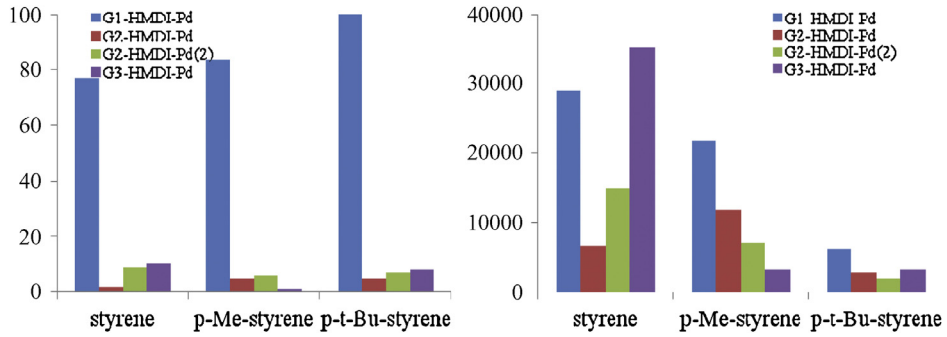

Fig. 24. The effect of the dendrimer generation on (a) the conversion and (b) the hydrogenation activity of the substrate over palladium catalysts with the HMDI cross-linker. Reaction conditions: (1) styrene: 0.67 mg of the cat., 1 mL substrate, 80 °C, 15 min, 5 atm H_2; (2) p-Me-styrene: 0.83 mg cat., 1 mL substrate, 80 °C, 15 min, 5 atm H_2; (2) p-t-Bu-styrene: 2.5 mg cat., 1 mL of the substrate, 80 °C, 15 min, 5 atm H_2.

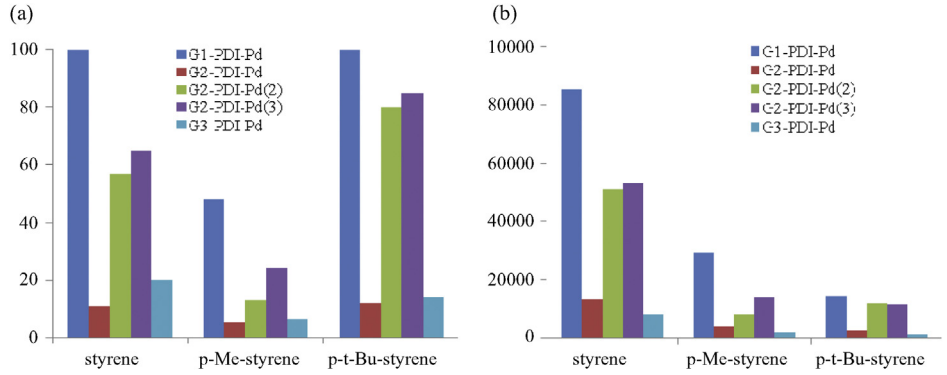

Fig. 25. The effect of dendrimer generation on (a) the conversion and (b) the hydrogenation activity of a substrate for palladium catalysts with the PDI cross-linker. Reaction conditions: (1) styrene: 0.67 mg of the cat., 1 mL of the substrate, 80 °C, 15 min, 5 atm H_2; (2) p-Me-styrene: 0.83 mg of the cat., 1 mL of the substrate, 80 °C, 15 min, 5 atm H_2; (2) p-t-Bu-styrene: 2.5 mg of the cat., 1 mL of the substrate, 80 °C, 15 min, 5 atm H_2.

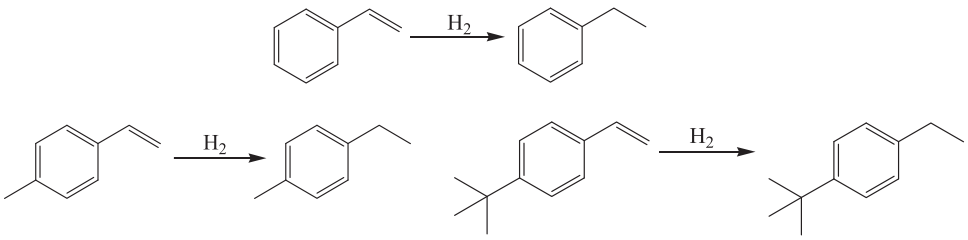

Scheme 4. The hydrogenation of styrene to form the corresponding alkyl benzenes.

$G_3$2-PDI-Pd catalysts, which contain a phenyl ring, p-phenylene and 3,3′-dimethoxy-4,4′-diphenylene diisocyanate are used as the cross-linkers, and a parabolic dependence on the value of the alkyl substituent para to the vinyl group of styrene is also typical. The maximum activity is achieved during the hydrogenation of p-tert-butylstyrene (Fig. 25a).

A similar dependence between the PAMAM dendrimer generation and the PDI cross-linker is shown in Fig. 25. Therefore, the catalysts containing p-phenylene diisocyanate as a linker hydrogenate p-methylstyrene poorly, while the conversion for the hydrogenation of styrene and p-tert-butylstyrene exceeds 60% for the G1-PDI-Pd, $G_2$2-PDI-Pd and $G_3$2-PDI-Pd catalysts. As observed in this graph, the Pd content does not affect the conversion: the Pd contents in the G1-PDI-Pd and G3-PDI-Pd samples are 15.83% and 13.73%, respectively, and the conversions of styrene are 100% and 20%, respectively. This effect can be explained by the surface atomic concentration of palladium because, in the second sample, little palladium is located at the surface (Table 1). The lowest activity is exhibited by all catalysts containing this active cross-linking agent during the hydrogenation of p-tert-butylstyrene (Fig. 25a).

The substrate-dependence of conversion during hydrogenation using catalysts based on the first-generation PAMAM dendrimer with various cross-linking agents is shown in Fig. 25a. The worst conversion is observed with the G1-OMDI-Pd sample. When

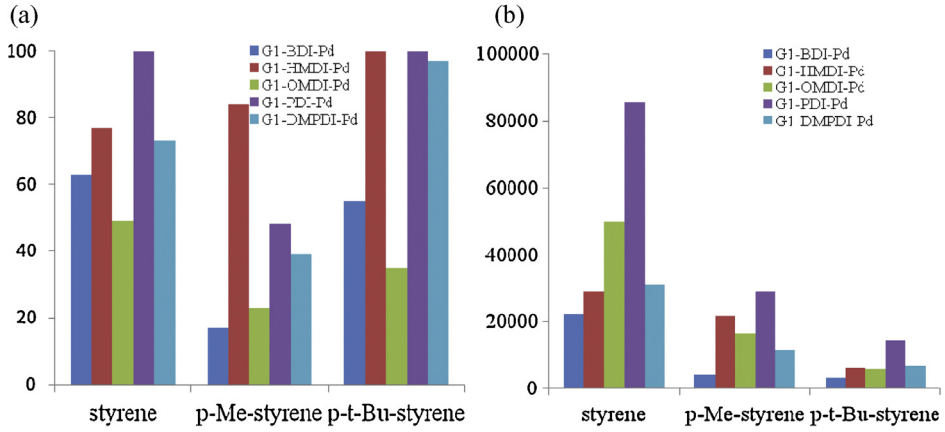

Fig. 26. The effect of the cross-linking agent on (a) the conversion and (b) the hydrogenation activity of the substrate over the palladium catalysts. Reaction conditions: (1) styrene: 0.67 mg of the cat., 1 mL of the substrate, 80 °C, 15 min, 5 atm H_2; (2) p-Me-styrene: 0.83 mg of the cat., 1 mL of the substrate, 80 °C, 15 min, 5 atm H_2; (2) p-t-Bu-styrene: 2.5 mg cat., 1 mL of the substrate, 80 °C, 15 min, 5 atm H_2.

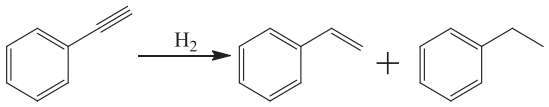

Scheme 5. The hydrogenation of phenylacetylene to form styrene and ethylbenzene.

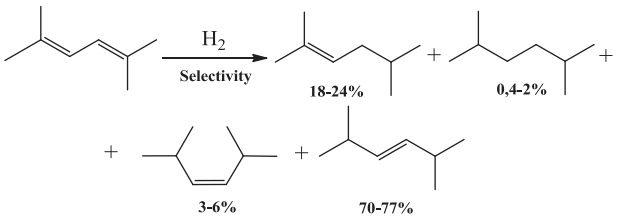

Scheme 6. Hydrogenation of 2,5-dimethyl-2,4-hexadiene.

comparing catalysts, the cross-linking agents that were conformationally flexible linkers such as the BDI, HMDI and OMDI were the best. A high conversion was achieved when using the G1-HMDI-Pd sample due to its superior pore structure; the pores facilitate the approach of the styrene toward the catalytic substrate. In addition, the palladium content does not affect the conversion (Fig. 25a). When using rigid linkers such as PDI and DMPDI, the best result was observed with the G1-PDI-Pd sample, where the Pd content is twice that in the G1-DMPDI sample.

A similar situation is observed when considering the activity of the catalyst based on the first-generation PAMAM dendrimer with various cross-linking agents (Figs. 24b and 25b). These samples are the least active toward the hydrogenation of p-tert-butylstyrene due to steric hindrance. Apparently, the optimal substrate size corresponds to the distance between the branches of the dendritic matrix. During the hydrogenation of styrene, the catalyst activity decreases in the following order: G1-PDI-Pd » G1-OMDI-Pd > G1-DMPDI-Pd > G1-HMDI-Pd > G1-BDI-Pd (Fig. 26b).

3.5.3. *Hydrogenation of phenylacetylene*

During the hydrogenation of phenylacetylene (Scheme 5) over 15 min, 100% conversion is achieved when using two catalysts: G1-HMDI-Pd and G1-BDI-Pd (Table 2). G1-PDI-Pd achieves a 98% conversion. These high conversions may be attributed to the higher flexibility of the cross-linking agents. The palladium content exerts no effect on the conversion of phenylacetylene; the conversions of the G1-HMDI-Pd and G1-PDI-Pd samples are 14.8% and 6.8%, respectively. The G2-HMDI-Pd, G3-HMDI-Pd and $G_2$2-PDI-Pd samples produce the worst results with 17%, 11% and 15% conversion, respectively. Therefore, the conversion decreases when increasing the dendrimer generation: G1-HMDI-Pd » G2-HMDI-Pd > G3-HMDI-Pd. The same trend is observed when using catalysts with the PDI cross-linking agent: G1-PDI-Pd » $G_2$2-PDI-Pd. All of the samples were selective with respect to styrene except the G1-DMPDI-Pd and $G_2$2-PDI-Pd samples. The hydrogenation of phenylacetylene over these catalysts generates ethylbenzene quantitatively; this result may be explained by the rigid cross-linkers.

During the hydrogenation of phenylacetylene over 1 h using catalysts based on the first generation dendrimers with different cross-linkers, 100% conversion is achieved with a 99% selectivity for styrene when using G1-PDI-Pd (Table 2). When hydrogenating styrene and its derivatives, the results depend on the optimal average palladium particle size (2.5 nm). When hexamethylene is used as a cross-linker, the selectivity is 0%; specifically, the hydrogenation runs to completion, forming ethylbenzene in a 100% yield. The hydrogenation is not affected by the palladium content when using catalysts based on the first-generation dendrimer.

The G1-DMPDI-Pd and $G_2$2-PDI-Pd catalysts are the least selective toward styrene (the selectivity is 11%), similar to the phenylacetylene hydrogenation that occurred over 15 min.

The G2-HMDI-Pd and G3-HMDI-Pd catalysts had similar palladium contents: 1.61% and 1.66%, respectively. These materials hydrogenate phenylacetylene with almost the same yield and selectivity. Therefore, the dendrimer generation does not affect the conversion and selectivity.

The best catalyst for phenyl acetylene hydrogenation is G1-HMDI-Pd, with 100% yield of styrene being formed in the reaction for 15 min, and 100% yield of ethylbenzene is produced in the reaction for 1 h. The most active catalyst is the G1-PDI-Pd, with a TOF of $14.5 \times 10^3\ h^{-1}$ in the hydrogenation of phenyl acetylene for 15 min; using G2-PDI-Pd, the TOF is $13 \times 10^3\ h^{-1}$ in hydrogenation for 1 h.

3.5.4. *Hydrogenation of 2,5-dimethyl-2,4-hexadiene*

During the hydrogenation of 2,5-dimethyl-2,4-hexadiene, four products were obtained: 2,5-dimethyl-hexane, 2,5-dimethyl-2-hexene, 2,5-dimethyl-3(trans)-hexene, and 2,5-dimethyl-3(cis)-hexene (Scheme 6). All of the catalysts were selective toward 2,5-dimethyl-3(trans)-hexene with selectivities ranging from 70 to 77% (Table 3). The table shows that the selectivity for 2,5-dimethyl-hexane ranges from 0.4 to 2.5%. The selectivity for 2,5-dimethyl-3(cis)-hexene ranges from 3 to 6%, while that of 2,5-dimethyl-2-hexene ranges from 18 to 24%.

Table 2
Hydrogenation of phenylacetylene in the presence of Pd catalysts based on dendrimers.

No.	Catalyst	Conversion % (15 min)	Selectivities, % (15 min)	TOF (h^{-1})	Conversion % (1 h)	Selectivities, % (15 min)	TOF (h^{-1})
1	G1-BDI-Pd	100	78	6112	100	64	1548
2	G1-HMDI-Pd	100	100	6534	100	0	1634
3	G1-OMDI-Pd	19	82	6746	28	80	2248
4	G1-PDI-Pd	98	95	14580	100	99	3720
5	G1-DMPDI-Pd	67	0	4911	100	11	1251
6	G2-HMDI-Pd	17	91	9849	60	94	3189
7	G2-PDI-Pd	64	82	26863	85	94	12935
8	$G_2$2-HMDI-Pd	25	88	7264	58	88	4267
9	$G_2$2-PDI-Pd	15	0	2329	51	11	2006
10	G2-DMPDI-Pd	74	98	17505	98	0	5870
11	G3-HMDI-Pd	11	95	6610	57	93	8413
12	G3-PDI-Pd	67	93	9442	100	100	3569

Reaction conditions: 4 mg of the catalyst per 1 mL of the substrate, 80 °C, 10 atm H_2.

Table 3
Hydrogenation of 2,5-dimethyl-2,4-hexadiene in the presence of Pd catalysts based on dendrimers.

No.	Catalyst	Conversion (%)	Selectivities, % 2,5-dimethyl-hexane	Selectivities, % 2,5-dimethyl-2-hexene	Selectivities, % 2,5-dimethyl-3(trans)-hexene	Selectivities, % 2,5-dimethyl-3(cis)-hexene	TOF (h^{-1})
1	G1-BDI-Pd	70	0.6	19	76	4	13176
2	G1-HMDI-Pd	54	0.6	20	74	5	10851
3	G1-OMDI-Pd	38	0.8	18	77	4	20778
4	G1-PDI-Pd	61	0.4	21	74	5	27966
5	G1-DMPDI-Pd	95	0.4	24	70	6	21578
6	G2-HMDI-Pd	9	2.5	19	75	3	16657
7	G2-PDI-Pd	7	2.3	22	74	1,7	4525
8	$G_2$2-HMDI-Pd	17	1.4	19	77	3	13352
9	$G_2$2-PDI-Pd	18	0.7	22	73	4	8610
10	$G_3$2-PDI-Pd	46	0.7	21	74	4	20159
11	G2-DMPDI-Pd	20	2.6	20	75	3,4	14572
12	G3-HMDI-Pd	11	2	20	75	3	19747
13	G3-PDI-Pd	12	1.3	21	75	2,7	2605

Reaction conditions: 1 mg of the catalyst per 1 mL of the substrate, 80 °C, 15 min, 10 atm H_2.

During the hydrogenation of 2,5-dimethyl-2,4-hexadiene using the catalysts based on the first-generation PAMAM dendrimer and various cross-linkers, the conversion decreases in the following order: G1-DMPDI-Pd > G1-BDI-Pd > G1-PDI-Pd > G1-HMDI-Pd > G1-OMDI-Pd. This trend may be related to the pore sizes of the cross-linked dendrimer, while the palladium content and particle size do not affect the conversion (Table 3).

When using the catalysts based on the PAMAM dendrimers with hexamethylene diisocyanate, the cross-linking agent conversion decreases in the following sequence: G1-HMDI-Pd » $G_2$2-HMDI-Pd > G3-HMDI-Pd > G2-HMDI-Pd. This trend may also be explained by the pore sizes. The difference in conversion between the G2-HMDI-Pd and G3-HMDI-Pd samples is only 2. Therefore, the conversion is affected by the palladium content.

When using catalysts based on the first- and second-generation PAMAM dendrimers with p-phenylene diisocyanate, the conversion decreases in the following sequence: G1-PDI-Pd » $G_3$2-PDI-Pd > $G_2$2-PDI-Pd. The effects of the palladium content and its surface atomic content on the activity of the catalyst are observed.

The most active catalyst during the hydrogenation of 2,5-dimethyl-2,4-hexadiene is the G1-PDI-Pd sample; its TOF was $28 \times 10^3\ h^{-1}$. The catalytic activity decreases in the following order: G1-PDI-Pd > G1-DMPDI-Pd > G1-OMDI-Pd » G1-BDI-Pd > G1-HMDI-Pd. This trend can be explained by the increased steric hindrance during substrate coordination. When using catalysts based on the first-, second- and third-generation PAMAM dendrimers with the HMDI cross-linker, the activity increases in the following order: G1-HMDI-Pd < $G_2$2-HMDI-Pd < G2-HMDI-Pd < G3-HMDI-Pd. When using the catalysts with the PDI linker, the catalyst activity decreases when increasing the PAMAM dendrimer generation.

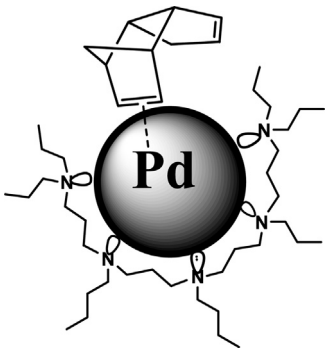

Fig. 27. DCPD adsorption on the Pd nanoparticles.

3.5.5. Hydrogenation of dicyclopentadiene

Materials based on dendrimer-encapsulated palladium nanoparticles are effective catalysts during the hydrogenation of dicyclopentadiene (Table 4). Five products are formed: the endo- and exo-isomers with small quantities of cyclopentadiene, cyclopentane and cyclopentene (Scheme 7).

During the hydrogenation, the configuration of the initial dicyclopentadiene (endo) is maintained, and the less sterically hindered and higher energy double bond is hydrogenated (Fig. 27), matching the published data [26]. The amount of diene decomposition products did not exceed 13% for G1-HMDI-Pd, G2-HMDI-Pd, G2-PDI-Pd, $G_2$2-HMDI-Pd, $G_2$2-PDI-Pd, and G3-HMDI-Pd. The amounts of decomposition were 21%, 37% and 31% for G1-BDI-Pd, G1-PDI-Pd and G1-DMPDI-Pd, respectively.

The highest hydrogenation conversions were 92% and 96% for the G1-HMDI-Pd and G1-PDI-Pd samples, respectively, due to their nearly identical particle sizes (2.1 and 2.49 nm). When using

Table 4
Hydrogenation of dicyclopentadiene in the presence of Pd catalysts based on dendrimers.

No.	Catalyst	Conversion, % (15 min)	% Percentage of decomposition	Internal conversion (%)	Endo/exo	TOF (h^{-1})
1	G1-BDI-Pd	78	21	79	7:1	7908
2	G1-HMDI-Pd	92	5	97	23:1	9982
3	G1-OMDI-Pd	17	9	18	6:1	5006
4	G1-PDI-Pd	96	37	98	16:1	24206
5	G1-DMPDI-Pd	61	31	89	10:1	7462
6	G2-HMDI-Pd	21	6	23	29:1	20934
7	G2-PDI-Pd	17	4	18	7:1	5918
8	$G_2$2-HMDI-Pd	26	7	28	28:1	12531
9	$G_2$2-PDI-Pd	79	13	91	61:1	20352
10	G2-DMPDI-Pd	73	0.06	74	39:1	28647
11	G3-HMDI-Pd	34	2	35	15:1	32873
12	G3-PDI-Pd	9	8	10	8:1	1052

Reaction conditions: 2 mg of the catalyst per 1 mg of the substrate, 80 °C, 15 min, 10 atm H_2.

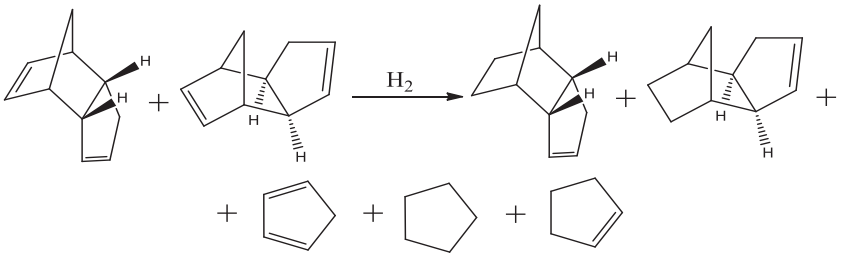

Scheme 7. The hydrogenation of dicyclopentadiene.

the first-generation catalysts with various cross-linkers, a relatively high conversion was achieved. The conversion increases in the following order based on the optimal particle sizes and palladium contents: G1-OMDI-Pd « G1-DMPDI-Pd < G1-BDI-Pd « G1-HMDI-Pd < G1-PDI-Pd. The major products underwent the hydrogenation of only one bond through the endo-isomer. The ratio of endo- to exo-products ranged from 7:1 to 23:1. Therefore, the specific activity of the catalysts increases.

When using the catalysts based on the first-, second- and third-generation dendrimers with the HMDI cross-linker, the yields increase in the following order due to the particle size and surface concentration of palladium: G2-HMDI-Pd < $G_2$2-HMDI-Pd < G3-HMDI-Pd « G1-HMDI-Pd. In addition, the conversion is affected by the dendrimer generation. The conversion while using the G3-HMDI-Pd sample exceeds that obtained while using G2-HMDI-Pd; the palladium contents of these samples are almost identical (1.61 and 1.66%, respectively), but the particle sizes are 1 92 nm and 1.74, respectively. The best selectivity is achieved by using G1-HMDI-Pd and $G_2$2-HMDI-Pd: 96% and 97%, respectively.

When using the catalysts based on the first-, second- and third-generation dendrimers with the PDI linker, the yields increase in the following order due to the palladium contents and surface palladium content: G2-PDI-Pd « $G_2$2-PDI-Pd < G1-PDI-Pd. This trend can be explained by the average particle sizes: 1.07 and 1.46 nm for G2-PDI-Pd, 1.09 and 1.89 nm for $G_2$2-PDI-Pd and 2.49 nm for G1-PDI-Pd. The last sample is optimal in that the highest conversion is achieved while using this sample. $G_2$2-PDI-Pd exhibits the highest selectivity (98%). Similarly, the specific activity and the conversion of the catalysts varies. The worst catalyst during the hydrogenation of dicyclopentadiene is G2-PDI-Pd because the average particle size (1.07 and 1.46 nm) is far from the optimal range (2.1–2.5 nm).

4. Conclusions

Therefore, using nanostructured entities based on cross-linked dendrimers and palladium nanoparticles allows the synthesis of highly active and selective catalysts for the hydrogenation of unsaturated compounds. The activity and selectivity of these systems depended on the nature and the structure of the dendritic matrix, as well as its affinity to the substrate. The maximal yields and activities are achieved during the hydrogenation of styrene to form the corresponding ethyl benzene.

Acknowledgments

This work was supported by RFBR Grant no. 14-03-3153-A.

References

[1] R.A. Findeis, L.H. Gade, Eur. J. Inorg. Chem. (2003) 99–110.
[2] V. Marval, A.M. Caminade, J.P. Majoral, Organometallics 19 (2000) 4015.
[3] L. Ropartz, R.E. Morris, D.F. Foster, D.J. Cole-Hamilton, Chem. Commun. (2001) 361–362.
[4] Y. Ribourdouille, G.D. Engel, M. Richard-Plouet, L.H. Gade, Chem. Commun. (2003) 1228–1229.
[5] S. Antebi, P. Arya, L.E. Manzer, H. Alper, J. Org. Chem. 67 (2002) 6623–6631.
[6] M. Pittelkow, K. Moth-Poulsen, U. Boas, J.B. Christensen, Langmuir 19 (2003) 7682–7684.
[7] E.H. Rahim, F.S. Kamounah, J. Frederiksen, J.B. Christensen, Nano Lett. 1 (9) (2001) 499–501.
[8] K. Heuze, D. Mery, D. Gauss, J.-C. Blais, D. Astruc, Chem. Eur. J. 10 (2004) 3936–3944.
[9] T. Borkowski, P. Subik, A.M. Trzeciak, S. Wolowiec, Molecules 16 (2011) 427–441.
[10] E.A. Karakhanov, A.L. Maksimov, A.V. Zolotukhina, Y.S. Kardasheva, Russian Chem. Bull. 62 (7) (2013) 1465–1492.
[11] E.A. Karakhanov, A.L. Maximov, Y.S. Kardasheva, V. Semernina, A.V. Zolotukhina, A.O. Ivanov, G. Abbott, E. Rosenberg, V. Vinokurov, ACS Appl. Mater. Interf. 6 (10) (2014) 8807–8816.
[12] K. Olofsson, C.J. Andren, M. Malkoch, J. Appl. Polym. Sci. 131 (3) (2014) 39876.
[13] Y. Niu, R.M. Crooks, C.R. Chimie 6 (2003) 1049–1059.
[14] M. Bernechea, E. de Jesus, C. Lypez-Mardomingo, P. Terreros, Inorg. Chem. 48 (2009) 4491–4496.
[15] D. Bharathi, A.H. Ronald, M. de V Melgardt, Int. J. Pharm. 284 (2004) 133–140.
[16] Y. Niu, L. Sun, R.M. Crooks, Macromol. 36 (2003) 5725–5731.
[17] S.-K. Oh, Y. Niu, R.M. Crooks, Langmuir 21 (2005) 10209–10213.
[18] R. Andres, E. de Jesus, J.C. Flores, New J. Chem. 31 (2007) 1161–1191.
[19] E.A. Karakhanov, A.L. Maximov, V.A. Skorkin, A.V. Zolotukhina, A.S. Smerdov, A.Y. Tereshchenko, Pure Appl. Chem. 81 (11) (2009) 2013–2023.

[20] E.A. Karakhanov, A.L. Maksimov, A.V. Zolotukhina, S.V. Kardashev, Petroleum Chem. 50 (4) (2010) 290–297.
[21] E.A. Karakhanov, A.L. Maximov, S.V. Kardashev, Y.S. Kardasheva, A.V. Zolotukhina, E. Rosenberg, J. Allen, Macromol. Symp. 304 (1) (2011) 55–64.
[22] E.A. Karakhanov, A.L. Maksimov, A.V. Zolotukhina, S.V. Kardashev, T. Yu Filippova, Petroleum Chem. 52 (5) (2012) 289–298.
[23] W. Soichiro, I. Michiko, J. Photochem. Photobiol. A: Chem. 155 (2003) 57–62.
[24] R.M. Crooks, M. Zhao, L. Sun, V. Chechik, L.K. Yeung, Acc. Chem. Res. 34 (2001) 181–190.
[25] NIST. Electronic data base of the XPS. http://srdata.nist.gov/xps
[26] M. Hao, B. Yang, H. Wang, G. Liu, S. Qi, J. Yang, Ch. Li, J. Lu, J. Phys. Chem. A 114 (11) (2010) 3811–3817.